JNeurosci Accepted Manuscript

JNeurosci
THE JOURNAL OF NEUROSCIENCE

Research Articles: Development/Plasticity/Repair

Age-dependent remarkable regenerative potential of the dentate gyrus provided by intrinsic stem cells

https://doi.org/10.1523/JNEUROSCI.1010-19.2019

Cite as: J. Neurosci 2020; 10.1523/JNEUROSCI.1010-19.2019

Received: 5 May 2019
Revised: 11 December 2019
Accepted: 12 December 2019

This Early Release article has been peer-reviewed and accepted, but has not been through the composition and copyediting processes. The final version may differ slightly in style or formatting and will contain links to any extended data.

Alerts: Sign up at www.jneurosci.org/alerts to receive customized email alerts when the fully formatted version of this article is published.

Copyright © 2020 the authors

JNeurosci Accepted Manuscript

Age-dependent remarkable regenerative potential of the dentate gyrus provided by intrinsic stem cells

Abbreviated title: Dentate gyrus regeneration after massive destruction

Tamar Licht[1,3#], Tirzah Kreisel[1,2], Yoav Biala[3], Sandesh Mohan[3], Yoel Yaari[3,] Andrey Anisimov[4], Kari Alitalo[4] and Eli Keshet[1#]

[1]Dept. of Developmental Biology and Cancer Research, Faculty of Medicine, the Hebrew University, Jerusalem 91120 Israel.

[2]Edmond and Lily Safra Center for Brain Sciences (ELSC), The Hebrew University Givat Ram, Jerusalem 91904.

[3]Dept. of Medical Neurobiology, Faculty of Medicine, the Hebrew University, Jerusalem 91120 Israel.

[4]Translational Cancer Biology Program, Research Programs Unit, Faculty of Medicine, University of Helsinki, Finland FI-00014

Corresponding authors

Tamar Licht: mail: tamarli@ekmd.huji.ac.il. Phone 972544703220. Fax 97226757195

Eli Keshet: elik@ekmd.huji.ac.il. Phone 972524634418. Fax 97226757195

No. of pages: 36

No. of figures: 10

No. of tables: 1

Words in abstract: 216

Words in introduction: 631

Words in discussion: 880

The authors declare no competing financial interests.

JNeurosci Accepted Manuscript

Acknowledgments

This work was supported by a European Council Research (ERC) grant; project VASNICHE (Grant # 322692). We thank Steffen Jung (The Weizmann Institute), Grigori Enikolopov (CSHL), Rudolf Jaenisch (MIT) for mice and Alissa Greenwald and Brachi Wolf (HU) for assistance.

Abstract

Multiple insults to the brain lead to neuronal cell death, thus raising the question to what extent can lost neurons be replenished by adult neurogenesis. Here we focused on the hippocampus and especially the dentate gyrus (DG), a vulnerable brain region and one of the two sites where adult neuronal stem cells (NSCs) reside. While adult hippocampal neurogenesis was extensively studied with regard to its contribution to cognitive enhancement, we focused on their underestimated capability to repair a massively injured, nonfunctional DG. To address this issue, we inflicted substantial DG-specific damage in mice of either sex either by diphtheria toxin-based ablation of >50% of mature DG granule cells (GCs) or by prolonged brain-specific VEGF overexpression culminating in extensive, highly selective loss of DG GCs (thereby also reinforcing the notion of selective DG vulnerability). The neurogenic system promoted effective regeneration by increasing NSCs proliferation/survival rates, restoring a nearly original DG mass, promoting proper rewiring of regenerated neurons to their afferent and efferent partners and regaining of lost spatial memory. Notably, concomitantly with the natural age-related decline in the levels of neurogenesis, the regenerative capacity of the hippocampus also subsided with age. The study thus revealed an

JNeurosci Accepted Manuscript

unappreciated regenerative potential of the young DG and suggests hippocampal NSCs as a critical reservoir enabling recovery from catastrophic DG damage.

Significance statement

Adult hippocampal neurogenesis has been extensively studied in the context of its role in cognitive enhancement but whether, and to what extent can dentate gyrus (DG)-resident neural stem cells drive regeneration of an injured DG has remained unclear. Here we show that DG neurogenesis act to replace lost neurons and restore lost functions even following massive (>50%) neuronal loss. Age-related decline of neurogenesis is paralleled by a progressive decline of regenerative capacity. Considering also the exceptional vulnerability of the DG to insults, these findings provide a further rationale for maintaining DG neurogenesis in adult life.

JNeurosci Accepted Manuscript

Introduction

Stem cells in adult organs are engaged in homeostatic maintenance of the tissue, both in balancing normal cell turnover, as well as in tissue repair following injury.

In the brain, neural stem cells (NSCs) mostly reside in two locales: the sub-ventricular zone (SVZ) and the hippocampal dentate gyrus (DG). The major role of SVZ NSCs is the replenishment of olfactory bulb interneurons in compensation for their normal turnover. SVZ-born neuroblasts migrate rostrally to the olfactory bulb via a designated route known as the rostral migratory stream (RMS). While it was shown that SVZ-born neurons can use alternative routes and home to injured brain areas in models of stroke and ischemia (Nakatomi et al., 2002; Zhang et al., 2004; Grade et al., 2013), it is unclear whether they also contribute to functional repair (Inta and Gass, 2015; Lu et al., 2017).

DG-resident NSCs are engaged in constitutive production of new neurons in rodents and potentially also in humans (Eriksson et al., 1998; Spalding et al., 2013; Boldrini et al., 2018) that integrate within the existing network of DG granule cells (GCs) (van Praag et al., 2002) where they contribute to memory and mood processes (Aimone et al., 2011; Toda et al., 2018). Although neurogenic response was documented in experimental animal models of injury and epilepsy (Gould and Tanapat, 1997; Gray and Sundstrom, 1998; Jessberger et al., 2007; Cho et al., 2015; Yu et al., 2016), the natural role of NSCs in functional DG repair following injury is grossly underappreciated. This issue is of particular significance given the vulnerability of the hippocampus, in general, and of GCs in particular, to damaging insults. Owing to the low excitability of GCs and their natural role in moderation of excitatory signals (Heinemann et al., 1992; Krook-Magnuson et al., 2015), their loss is a major cause of temporal lobe epilepsy, a pathology further aggravating selective GC loss and often culminating in DG degeneration (Houser, 1992; Steward, 1994). Examining whether DG NSCs are capable of driving functional DG repair in epilepsy models has been hampered by the continual nature of the damage counteracting the repair process (Hattiangady et al., 2004). Likewise, DG

JNeurosci Accepted Manuscript

neurogenesis induced by Kainic acid was shown to be associated with accelerated NSC depletion and astrocytic differentiation rather than neuron production (Sierra et al., 2015). The exceptional vulnerability of the DG is also evidenced in other human pathologies such as frontotemporal lobe degeneration, Alzheimer's disease and adrenal insufficiency (Maehlen and Torvik, 1990; Armstrong et al., 2012; Collins et al., 2012; Kovacs et al., 2013; Takeda and Tamano, 2018) and in rodent models of these and other pathologies that are often associated with enhanced neurogenesis (Spanswick et al., 2007; Spanswick et al., 2011; Watanabe et al., 2016; Choi et al., 2017; Tu et al., 2018; Wang et al., 2018).

To examine the regenerative potential of the DG we used two independent ways for conditional infliction of GC-specific massive cell death, importantly, under conditions sparing NSCs. In the first model, diphtheria toxin (DT) injected to adult mice expressing DT receptors exclusively in GCs leads to selective elimination of >50% of GCs. In the second model, a comparable GC-specific loss is caused by conditionally-induced prolonged (>3 months) overexpression of VEGF. Importantly, the damaging insult in this tetracycline-regulated VEGF system can be terminated at will, thus providing a unique opportunity to uncouple the processes of DG injury and repair. Here we uncovered a remarkable regenerative capacity of the DG, not only with respect to replenishing lost neurons but also with respect to proper re-wiring and restoration of lost cognitive functions. We further show that regeneration is driven by DG NSCs and that progressive neurogenesis decline with age (Kuhn et al., 1996; Ben Abdallah et al., 2010; Encinas et al., 2011) is accompanied by a progressive diminishment of the regenerative potential.

Materials and Methods

Mice

All animal procedures were approved by the animal care and use committee of the Hebrew University. Transgenic mouse lines that were used in this study: CamkIIα-tTA, Ai9, Pomc-Cre, iDTR,

JNeurosci Accepted Manuscript

and Gli1-cre^{ERT2} lines were purchased from the Jackson Laboratories (strains 016198, 007909, 010714, 007900, 007913). pTET-VEGF$_{164}$ and pTET-sVEGFR1 responder lines were as described previously (Licht et al., 2011). Nestin-GFP line was obtained from Prof. Grigori Enikolopov, CSHL (Mignone et al., 2004). pTET-GFP line was obtained from R. Jaenisch, MIT (Beard et al., 2006). Both males and females were used. For switching-off VEGF, water was supplemented by 500mg/L tetracycline (Bio Basic Canada Inc. #TB0504) and 3% sucrose. For switching on the transgene, tetracycline-supplemented water was replaced by fresh water for the desired time. CldU (MP Biomedicals #02105478 100mg/kg) or IdU (Sigma I7125, 100mg/kg) were injected intraperitoneally (i.p.) 3 times at 8hr intervals at the indicated time points. Tamoxifen (Sigma T5648, 40mg/ml in sunflower seed oil) was administered orally once daily for 5 days at a dose of ~8mg/animal. TRITC-labeled 10kD dextran (Molecular Probes #1817) was injected intracardially at 100gr/kg 2 min before sacrifice. Animals were grown in SPF housing conditions with irradiated rodent food and water/tetracycline ad libitum. Breeding cages for the VEGF system include males heterozygous for pTET-VEGF$_{164}$, CamkIIα-tTA and Ai9/nestin-GFP alleles and females heterozygous for CamkIIα-tTA and Gli1- creERT2/nestin-GFP (maternal imprinting of the pTET-VEGF$_{164}$ allele results in high mortality upon VEGF induction). Mice that inherited the CamkIIα-tTA alone served as controls for CamkIIα-tTA; pTET-VEGF$_{164}$ double transgenic littermates. All animals in experiments (controls and VEGF) were kept in the same cage and received the same treatment. Litters of either sex were used.

Intrahippocampal injections

Mice were anesthetized with an i.p injection of Ketamine/Xylazine followed by Isoflurane inhalation. The head was placed in a stereotactic apparatus (Stoelting Co.) and a burr hole was drilled at the injection site using the following coordinates relative to Bregma (in mm): AP: −2.5, ML: -1.4, DV: −2. Injections were conducted using a 10µl syringe (Hamilton) and a thin 33-gauge metal needle (WPI). DT (Merck Millipore, # 322326, 5µg/ml) or AAV-VEGF (3E+06vp/µl (Kivela et

JNeurosci Accepted Manuscript

al., 2019)) were dissolved in saline and 1µl was delivered at a flow rate of 0.4µl/min. After injection, the needle was left in place for 5 additional minutes and then slowly withdrawn. For bilateral injections (ML: ±1.4), a 0.7µl of DT in each hemisphere was administered. All mice received DT injections while mice inherited iDTR alone served as controls. For AAV experiment, an empty AAV vector served as control.

Electrophysiology

Mice were decapitated under Isoflurane anesthesia and coronal hippocampal slices (350µm) were prepared with a vibratome and transferred to a storage chamber perfused with oxygenated (95% O_2 and 5% CO_2) artificial cerebrospinal fluid (aCSF) at room temperature (containing (mM): NaCl 130; KCl 3.5; $MgSO_4$ 1; $CaCl_2$ 1.6; $NaHCO_3$ 24; and D-glucose, 10). For recording, slices were placed one at a time in an interface chamber and superfused (flow rate 1 ml/min) with warmed (35°C) oxygenated aCSF. The temperature was measured with a thermal probe juxtaposed to the slice and maintained at 35°C with a feedback controller (NPI, Tamm, Germany). Bipolar tungsten (115 µm) electrodes (FHC, Inc.) connected to a stimulator by an isolation unit were used for focal stimulation (1–20 V, 50 µs) of afferent fibers of Perforant path axons. Extracellular recordings were performed with glass electrodes contained 3M NaCl (5–10 MΩ), at the upper blade of the granule cell layer (GCL). An amplifier (EXT-10C, NPI electronic GmbH, Tamm, Germany) was used, allowing measurement of field potentials of cell populations. The extracellular signals were digitized at a sampling rate of 10 kHz and stored by a personal computer using a data acquisition system (Digidata 1322A) and pCLAMP9 software (Molecular Devices, CA). Each focal stimulation was performed 3-5 times, averaged, and the peak amplitude of the population spike was measured (from baseline to peak population spike).

Radial arm water maze

JNeurosci Accepted Manuscript

This protocol, testing for current working memory, was adapted from (Alamed et al., 2006; Fujisaki et al., 2014). The radial arm water maze apparatus of a circular pool (1M in diameter) with six 19cm wide arms radiating out from the central circular area. Visual cues were included in the test room. The experiment was conducted for 5 consecutive days. Escape transparent Plexiglas platform (16X16X20cm) was placed on a different arm each day (the platform location does not change over one day), forcing the mice to use their memory to solve the task. At the beginning of each acquisition trial, the animal was placed in a different arm out of the remaining arms not containing the escape platform on that day.

During each trial, the animal was allowed to swim into all arms until finding the platform. If during a 1 min trial the platform was not found, the mouse was gently guided through the water to the platform and was allowed to stay there for 10 sec. 30 min after finishing the 4th trial, each animal underwent a fifth trial with the start arm the same as that of trial 4.

The fifth trial on the fifth day was the "memory retention" trial, in which the number of errors to reach the platform were calculated. Each error was defined as either a) Swimming into an arm that does not contain the platform that day (1 error for every wrong arm entrance) b) Entering the goal arm without boarding the platform c) Spending 20 sec or more continuously in the central zone without any arm selection.

All trails were recorded and analyzed using EthoVision XT10 software (Noldus).

Immunohistochemistry

Brains were fixed by immersion in 4% PFA for 5 hrs., incubated in 30% sucrose, embedded in OCT Tissue-Tec and cryosectioned to 50µm floating sections. Coronal slices from all aspects of the rostral-caudal axis were examined.

Staining was done as described (Licht et al., 2010) with the following: anti-CldU (Serotec 1:400 PRID: AB_323427), anti-IDU (BD 1:200 PRID: AB_400326), anti laminin (Neomarkers 1:400 PRID: AB_60397), anti-DCX (Millipore 1:3000 PRID: AB_2230227) and anti-CD31 (BD 1:50 PRID:

JNeurosci Accepted Manuscript

AB_393571), anti NeuN (Cell Signaling 1:600 PRID: AB_2630395), anti ZnT3 (1:600, #AZT-013, Alomone labs) anti cleaved caspase 3 (1:200, Cell signaling PRID:AB_2341188), anti GFAP (1:500, Dako PRID: AB_10013482), anti Iba1 (1:200, Wako PRID: AB_2665520), anti HB-EGF for DTR (R&D, 1:200 PRID: AB_354429). Cy5 anti guinea-pig, Cy5 anti rat, Cy2 and Cy3 anti rabbit, Cy2 and Cy3-anti mouse were all obtained from Jackson Immunoresearch (dilution 1:400). Sections were mounted with Permafluor mounting medium (Thermo Scientific, TA-030-FM) with Dapi (Sigma, D9542).

Confocal microscopy was done using Olympus FV-1000 on 10X, 20X and X60 lenses and 1.46µm distance between confocal z-slices. Low magnification images were acquired using Nikon SMZ-25 stereoscope. At least 7 sections per animal from all hippocampal areas at the rostral-caudal axis were counted. Measurements were done using Olympus FV-1000 viewer.

DG size quantification

Measurements of the DG were performed as shown in Fig 1*H*. Coronal slices representing all areas of the hippocampus at the anterior-posterior axis were counted. **GCL area** was measured using X10 NeuN-stained sections by enclosing the GCL (using Olympus FV-1000 viewer) only in images including the GCL in full. **DG height** (Fig. 1*H* top, yellow) was measured as the distance in µm from the dorsal border with stratum lacunosum to the ventral border with the thalamus (yellow line in image). Measurements were done perpendicular to the center of the dorsal (suprapyramidal) blade. **GCL thickness** (Fig. 1*H* top, white*)* was measured at the center of the dorsal blade (white line). **MF thickness** (Fig. 1*H* bottom*)* was measured at the dorsal portion of CA3, at the level of the GCL dorsal blade ending (see red line in image). **CA1 height** (Fig. 4*C*) was measured from the dorsal border with the corpus callosum to the ventral border with stratum laconosum, perpendicular to the center of the pyramidal cell layer. Cells in the borders of ROI were included in analysis. All quantifications were done by a blind experimenter.

JNeurosci Accepted Manuscript

Cell density quantification

Since the total volume of the GCL was significantly lower in VEGF/DTR^{pomc} animals, cell numbers were normalized per SGZ area in 3d images, as this parameter did not change significantly in treated animals. The length of the SGZ (inner part of GCL) in every image was measured by Olympus FV-1000 viewer software using the Dapi channel. The area calculation was achieved by multiplying in the number of slices per image (usually 10-15) and the distance between slices (1.46µm). Quantification of cells within this area (DCX, CldU or IdU) was done manually using the same software by a blind experimenter.

To measure NeuN cell density, we encircled an area of 0.01µm^2 using Olympus FV-1000 viewer software and counted manually NeuN+ cells within the area in a single slice. Cells in the borders of the ROI were included in the analysis in all images.

Microvascular density (MVD) quantification

Z-stacks were processed by Bitplane IMARIS 7.6.3 software. An area of 318X318X22.5µm, including the hilus, GCL, and molecular layer, was analyzed. Surface function of the channel including blood vessel staining was conducted and the total volume was measured by IMARIS software (Detailed-average values-volume-sum). The ratio between blood vessel volume and the total ROI was calculated.

Experimental design and statistical analysis

Both males and females (from 1 or more litters per experiment) were used. The numbers of animals in each experiment, statistical tests and statistical values are summarized in *Table 1*. Graphs include the value per each animal and the mean ± SEM. Statistical comparisons were computed using SPSS 19.0 software and consisted of *t*-tests, one-way, two-way and repeated measure analyses of variance (ANOVAs), followed by the Tukey post hoc analyses. Prior to

JNeurosci Accepted Manuscript

statistical parametric tests, normality and homoscedasticity were assessed using the Shapiro-Wilk test and Levene's Test for Equality of Variances.

Results

Specific ablation of DG neurons in a Diphtheria-toxin-based inducible system.

With the aim of inflicting substantial neuronal loss, specifically of mature GCs, we used diphtheria toxin-based transgenic system in which Cre recombinase activity is driven by a POMC promoter previously shown to be specifically expressed in DG neurons (McHugh et al., 2007). Preparatory experiments using Ai9 TdTomato reporter validated that within the brain, POMC-Cre indeed drives expression of the reporter transgene robustly in the DG (see Fig. 1*A* for a scheme of transgenes used and Fig. 1*B* for results). Because the regenerative capacity of the DG assumedly relies on DG-resident NSCs, it was crucial to show that NSCs will be excluded from POMC-Cre-driven targeted transgenes. Visualizing NSCs with the aid of transgenic Nestin-GFP reporter, known to highlight radial glia-like (RGL) NSCs (Mignone et al., 2004), confirmed that this was indeed the case (Fig. 1*B,* right). Co-staining hippocampal sections for Doublecortin (DCX) to highlight differentiated neuroblasts showed that neuroblasts are also negative for Ai9 TdTomato (Fig. 1*C*), thereby securing that, unlike previously used DT-based neuronal ablation system causing widespread neuronal death (Yamasaki et al., 2007; Myczek et al., 2014), only mature GCs would be subjected to ablation with the aid of POMC-driven Cre recombinase.

To ablate GCs, POMC-Cre mice were crossed to mice harboring a Cre-inducible Diphtheria toxin receptor (iDTR) transgene (Fig. 1*D*) and double transgenic mice (dubbed DTR^{pomc} mice)

JNeurosci Accepted Manuscript

were challenged with Diphtheria toxin (DT) using unilateral intra-hippocampal stereotactic DT injection. Massive death of DG neurons was evidenced already by 5 days post-DT injection (5dpi), marked by DG-specific immunoreactivity for cleaved Caspase-3. Noteworthy, cleaved caspase-3 was not only detected in GC cell bodies but mostly in their dendrites extending to the adjacent molecular layer (ML) (Fig. 1*E* left). Apparent clustering of microglia in the granule cell layer (GCL) provided additional, indirect evidence for DG-specific cell damage (Fig. 1*E,* right).

The magnitude of the neuronal deficit was evaluated at 20 dpi where a marked reduction in overall DG cellularity was evident and calculated to comprise more than half of DG neurons (Fig. 1*F* left and middle and Fig. 1*H* for quantification). Mossy fiber (MF), the axonal tract extended by GCs, highlighted by immunostaining for the Zinc transporter ZnT3 (Palmiter et al., 1996), was also greatly reduced (Fig. 1*G,H*).

DG-resident NSCs drive full re-gain of lost neurons

The DT-based system of selective GC ablation described above provided us with a suitable platform for examining whether, and to what extent the DG can recover from such massive damage. To determine whether the substantial neuronal loss evidenced at 20 dpi can be repaired, and in order to allow sufficient time for regeneration, DT-treated brains of littermate mice were retrieved for analysis 70 days later (i.e., at 90 dpi). Remarkably, the neuronal deficit was found to be nearly fully rectified and the intact DG cellularity restored. This was evidenced in the restoration of normal DG height, GCL thickness, recovery of the MF and regaining the initial number of NeuN-positive DG neurons (Fig. 1*F-H*).

To determine whether this regenerative capacity is driven by resident NSCs, brains were retrieved for analysis at 20 dpi (Fig. 2*A*), i.e., the time point where substantial neuronal loss has already taken place and regeneration is ongoing. The assumption that NSCs will be spared in DT-injected DTR^{pomc} mice was validated by the observation that despite a massive DG

JNeurosci Accepted Manuscript

neuronal loss, the number of Nestin-GFP$^+$ NSCs was not reduced (Fig. 2*B*). Morphologically, RGL-type NSCs in DTR^{pomc} mice appeared to possess a major apical shaft and to lose the fine tree-like apical processes, a configuration previously shown to represent a reactive NSCs morphology (Sierra et al., 2015; Licht et al., 2016) (Fig. 2*B*, bottom). To follow the fate of dividing cells, the thymidine analog Chloro-deoxyuridine (CldU) was injected at 15-16 dpi, i.e., 4-5 days before brain retrieval. Intensive cell labeling was detected in the GCL of DTR^{pomc} mice compared to the low basal neurogenic level observed in control mice (Fig. 2*C*). A significant fraction of NSCs was labeled with CldU (cells identified as GFP$^+$/CldU$^+$) (Fig. 2*D*,*F*). Further support to the contention that regeneration is driven by local NSCs comes from the observation of discernible 'clones' composed of progenitors (cells with no radial shaft) clustered around a proliferating RGL-type NSC, all positive for CldU (Fig. 2*D* right). The total number of DCX+ neuroblasts, as well as the number of early neuroblasts (co-labeled with CldU), were also higher in DTR^{pomc} mice (Fig. 2*E,F*). Active neuroblasts appeared to lose their typical morphology and to cluster at aberrant locales (Fig. 2*E*), as was shown for epilepsy models (Jessberger et al., 2007). To show that neuroblasts eventually differentiate into mature neurons, CldU was pulse-labeled at 60dpi and CldU$^+$/NeuN$^+$ mature neurons were enumerated at 90 dpi (Fig. 2*G*). Results confirmed a dramatic increase in newly-added mature neurons in the regenerated DG (Fig. 2*H*). Taken together, these findings attest to the ability of DG NSCs to drive full recovery of the DG following a massive injury. It should be noted, however, that even though normal cellularity was achieved at 90 dpi, cleaved-caspase 3 and activated microglia were still evident in the DG, indicative of ongoing injury (Fig. 2*I*). We, therefore, sought an additional system where the damage and regeneration phases are completely uncoupled.

Inflicting DG-specific neuronal loss by long-term exposure to ectopic VEGF

JNeurosci Accepted Manuscript

To corroborate that the DG can recover from extensive damage associated with massive neuronal loss, we examined its regenerative potential following a DG-specific injury of a different nature.

To this end, we used a transgenic platform allowing for brain-specific induction of ectopic VEGF in a conditional and reversible manner. Briefly, the system used was a bi-transgenic mouse system composed of a tetracycline-regulated, CamkIIα promoter-trans-activator (CamkIIα-tTA 'driving' transgene (Mayford et al., 1996) and a tet-$VEGF_{165}$ 'responder' transgene (Fig. 3*A*). This system was previously used by us to uncover a role for VEGF in reversible modulations of neuronal plasticity (Licht et al., 2011) and a role in the enhancement of adult hippocampal neurogenesis (Licht et al., 2016), but was later found to be associated with a substantial DG-specific damage whenever ectopic VEGF over-expression continued for a period exceeding two months. In our previous studies, VEGF was induced for up to one month, a period proven sufficient for eliciting sustained neurogenic enhancement, and then de-induced, conditions under which no hippocampal damage could be detected (Licht et al., 2016).

Here, VEGF induction was extended for a period of several months, conditions under which excessive VEGF led to not only angiogenic and neurogenic responses but was also associated with substantial selective DG damage underscoring the exceptional vulnerability of the DG (see below).

The nature and selectivity of DG injury

To evaluate the magnitude of VEGF-induced damage, VEGF was induced in mature 2 month-old CamkIIα-tTA: tet-VEGF double transgenic mice and continuously kept in the 'VEGF-ON' mode. Brains retrieved at monthly intervals (Fig. 3*B*) were sectioned and immunostained for the neuroblast marker DCX (Fig. 3*C*) and for the pan-neuronal marker NeuN (Fig. 3*D*). Results showed an enhanced neurogenic response that persists for several months (when natural

JNeurosci Accepted Manuscript

neurogenesis subsided with age) and ceased only by 7 months from the onset of VEGF overexpression (Fig. 3*C*). Concomitantly, there was a substantial, progressive reduction in the number of detectable mature DG neurons (Fig. 3*D*).

We wished to examine whether the detrimental response to VEGF is region-specific. With the aid of tet-GFP responder mouse (Fig. 4*A*), we aimed to examine the expression pattern dictated by the CamKIIα-tTA driver line. We were able to demonstrate a higher GFP expression in the CA1 in comparison with the DG (right). Similarly, using the TET-VEGF as a responder line (induced for 4 months), we showed that endothelial cells of the CA1 and the DG were equally responsive to VEGF - as judged by a comparable angiogenic response elicited by VEGF in both DG and CA1 (Fig. 4*B*). However, only the former showed clear evidence of neuronal damage due to the observation that the CA1 pyramidal cell density and height did not decrease (Fig. 4*C*). These findings reinforce the notion of exceptional DG vulnerability in comparison to other regions of the hippocampus. A further indication for the DG-specific VEGF-induced toxicity was apparent DG-restricted caspase-3 activation (Fig. 4*D* top, shown for the whole brain) and, indirectly, also DG-specific astrogliosis and microgliosis manifested in clustering of astrocytes and microglia in the injured DG but not in the CA1 (Fig. 4*D* middle and bottom). The kinetics of activation cleaved caspase 3, astrocytes and microglia after 1 and 3 months of VEGF induction are presented in Fig. 4*E*. While caspase 3 and astrocytes are highly activated only at 3 months from VEGF induction, microglia are activated at an earlier time point. Active microglia populate the DG specifically, as early as 3 days from VEGF induction (Kreisel et al., 2018) and may serve as the trigger for the selective response of the DG to VEGF.

VEGF is known as a neuroprotective agent (Jin et al., 2000; Oosthuyse et al., 2001). Here we show that under certain conditions, VEGF could become neurotoxic. The mechanism for GCs-selective neurotoxicity is not clear. The possibility that DG degeneration is secondary to excessive VEGF-induced vascular leakage was ruled out this option by showing that blood vessels in the DG are not leaky (Fig. 5*A*). Likewise, the possibility that the CamkIIα-tTA

JNeurosci Accepted Manuscript

transgene employed may on its own induce DG degeneration (Sirerol-Piquer et al., 2011; Han et al., 2012; Melnikova et al., 2016; Watanabe et al., 2016; Kukreja et al., 2018) was ruled out by showing that without the VEGF-responder transgene no damage was incurred (Fig. 5*B-D*). Also, DG degeneration and enhanced ectopic neurogenesis were reproduced using Intrahippocampal injection of VEGF-encoding Adeno-associated virus (AAV) (Fig. 5*E*).

Re-gain of normal DG cellularity and morphological features following VEGF withdrawal. In light of our findings that DG regeneration in the DT model relies on NSC-driven neurogenesis (Fig. 2), together with findings that DG neurogenesis in rodents precipitously declines with age (Ben Abdallah et al., 2010; Encinas et al., 2011), the time point of 3 months post-VEGF induction was selected as the 'baseline' for repair (Fig. 6). As in the DTR^{pomc} model, neuronal loss was measured as reduced GCL thickness, reduced density of $NeuN^{+}$ neurons, DG height (which includes also the space occupied by GC dendrites and axons) and MF thickness. Three months after continual VEGF exposure, GCL thickness was reduced by more than 60% and the density of GCL cell bodies and the total height of the DG by 40% (Fig. 6*B,D*). The thickness of the MF layer (visualized by ZnT3 immunostaining) was also dramatically reduced (Fig. 6*C,D*).

To examine the regenerative potential of the injured DG, the damaging insult was terminated by 'switching-off' VEGF (re-addition of tetracycline to the drinking water). On the basis of our previous studies showing that VEGF levels in brain parenchyma return to basal low levels within a couple of weeks from tetracycline addition (Licht et al., 2011), and to allow sufficient time for regeneration, brains were retrieved for analysis 3 months after VEGF de-induction (on>off, Fig. 6*A*). As shown in Fig. 6*B-D*, the neuronal deficit was repaired in the majority of animals in this timeframe and normal DG cellularity was nearly fully regained. MF, barely detectable in the injured DG, was found to be restored in many (but not all) cases (Fig. 6*C,D*). The magnitude of recovery was assessed by measuring the GCL area in NeuN-stained sections

JNeurosci Accepted Manuscript

at different time points during recovery. The graph presented in Fig. 3*D* is shown again with the on>off group (Fig. 6*E*). All damage-associated markers (e.g cleaved-caspase 3, active microglia and astrogliosis) were barely detected after 3 months of VEGF withdrawal (Fig. 4*E,* bottom).

Changes in neurogenesis rate and differentiation during degeneration and regeneration

VEGF-induced neurogenesis during degeneration (3m on) and regeneration (3m on/2m off) was examined at the level of NSCs with the aid of Nestin-GFP mice. Iodo-deoxyuridine (Melander et al.) was injected 1-2 days before brain retrieval (Fig. 7*A*). While the total numbers of NSCs were slightly reduced in the degenerated DG (Fig. 7*B* and Fig. 7*D*, left), the numbers of active (IdU+) NSCs were significantly higher in both 'on' and 'on>off' groups (Fig. 7*C,D*). In the control DG, NSCs appear as typical tree-like cells and their apical processes are associated with blood vessels (Fig. 7*B*, bottom images) (see further data for NSC-BV association in (Licht and Keshet, 2015; Moss et al., 2016)). In both 'on' and 'on>off' groups, NSCs acquire a modified morphology, lose the majority of the apical fine processes (their apical major shaft still in contact with blood vessels) (Fig. 7*B*, insets and Fig. 7*C*) and also send some cellular projections into the hilus (Fig. 7*C*). Modification of NSCs morphology was reported earlier to be associated with Kainic-acid treatment (reactive-type NSCs) (Sierra et al., 2015).

To reconcile the seemingly paradoxical situation of a higher rate of neuroblast production and yet progressive decrease in the number of mature DG neurons, we measured the fraction of newborn neuroblasts eventually differentiating into mature neurons. To this end, 3 months from the onset of VEGF induction mice were pulse-labeled with CldU and sacrificed 3 weeks thereafter in order to allow sufficient time for newborn neuroblasts to differentiate into mature NeuN+ neurons (Fig. 8*A*,*B*). Unlike a higher (~5 fold) rate of NSCs divisions (Fig. 7*D*) and similar increase in neuroblast production (DCX^+ cells, Fig. 8*C*), the number of newly-added

JNeurosci Accepted Manuscript

mature neurons was marginal (1.37-fold more $CldU^+/NeuN^+$ cells in 3m on mice, Fig. 8*B*), suggestive of non-productive neurogenesis in which only a minor fraction of neuroblasts eventually mature. Another indication of aberrant neurogenesis was that resembling the situation in epilepsy models, (Jessberger et al., 2007; Cho et al., 2015), DCX^+ cells were found in ectopic locations such as in the inner molecular layer and the hilus (Fig. 8*C,* insets). Interestingly, neurogenesis during the repair phase continued at the same high rate observed prior to VEGF de-induction, quantified through enumeration of both proliferating NSCs and DCX^+ neuroblasts as 4-fold higher than neurogenesis in non-injured littermate controls (Fig. 7*D* and Fig. 8*C*, respectively). However, unlike non-productive neurogenesis under prolonged, ongoing VEGF over-expression, neuroblasts generated during the repair period survived and successfully differentiated to mature $NeuN^+$ neurons. This was evidenced in a ~4-fold increase of CldU+NeuN+ cells compared to control or VEGF-on animals (Fig. 8*B*).

We measured the numbers of 3-weeks old DCX cells ($CldU^+DCX^+$), a population of late neuroblasts entering the final step of differentiation (Fig. 8*D*). This population was proportional to the total numbers of DCX cells in all groups, leading to the conclusion that newborn GCs are eliminated in the VEGF-on group subsequent to the DCX^+ stage.

An additional indication that prolonged VEGF exposure results in aberrant neurogenesis was obtained by following NSC descendants using lineage tracing. Briefly, NSCs were marked by crossing Gli1-Cre^{ERT2} mice (Ahn and Joyner, 2004) with a floxed- Ai9 TdTomato reporter mice and bred onto the VEGF switchable system (Fig. 8*E-H*). NSCs and their descendants were then visualized at different time points post VEGF induction and tamoxifen administration (short tamoxifen pulse highlight NSCs while longer tamoxifen pulses highlight their descendants). Results showed that while at 1.5 months after VEGF induction, newborn GCs with normal appearance were still observed (Fig. 8*G*, section iii), 1.5 months later, normal GCs were no longer detected. Instead, cells projecting to unusual areas and abnormal cells devoid of dendritic spines and even cells with no projections were evident (Fig. 8*G* section iv). Also,

JNeurosci Accepted Manuscript

NSCs discernible by their radial morphology acquire the modified morphology in the sense of losing the apical fine processes and projecting some distal processes into the hilus in addition to the molecular layer to where they are normally directed (Fig. 8*G*, sections iii, v, vii, and Fig. 7*C*). Newly-formed GCs in the regenerated DG, visualized through lineage tracing as above, were shown to have normal morphology marked by proper development of dendritic spines, indicative of synapse formation (Fig. 8*G* sections vi, vii). We summarized the relative numbers of NSC/GC normal and abnormal morphology of every experimental group in Fig. 8*H*. Together, findings suggest that neurogenesis in the repair phase is productive and has the capability of replacing lost neurons by the addition of newborn GC.

DG regeneration is marked by the restoration of functional GCs connectivity and re-gain of impaired learning and memory.

We have shown that newborn GCs during regeneration ('on>off') have a properly-oriented MF and dendrites comprising dendritic spines, indicative of new synapse formation (Fig. 8*G* sections vi, vii). To determine whether regenerated GCs (as in the protocol illustrated in Fig. 9*A*) re-establish lost functional connections, we examined perforant path connectivity, i.e., the pathway connecting afferent entorhinal cortex with the DG and also constituting the major input pathway to the DG. To this end, afferent fibers of the perforant path were stimulated in acute coronal hippocampal slices and excitatory postsynaptic potential (EPSP) was recorded in GCs located at the upper blade of the DG (Fig. 9*B*). A typical 1.5mV EPSP measured in the non-injured DG was found to be reduced to 0.2 mV by the end of the 3-month exposure to VEGF, indicating a barely functional perforant path. Regeneration led to partial but highly significant perforant path recovery measured as 0.6mV EPSP and a response curve resembling intact DG (Fig. 9*C,D*). Together with findings that all measured EPSP responses were inhibited by the glutamatergic inhibitors APV and CNQX (data not shown), we conclude that regenerated DG GCs establish functional glutamatergic synapses with entorhinal cortex neurons.

JNeurosci Accepted Manuscript

Anticipating that a DG damage of the magnitude shown in the 'VEGF-on' mice will lead to a significant cognitive deficit, we examined whether the anticipated cognitive loss is rectifiable by DG regeneration. To this end, mice were subjected to a radial arm water maze (RAWM) test (Alamed et al., 2006; Fujisaki et al., 2014). Briefly, mice were first trained daily for 5 consecutive days to locate a submerged platform hidden in one of the arms and their learning and memory skills were tested by determining the number of trial-and-error attempts required to find the hidden platform. Each mouse was trained and tested three times: before VEGF induction, 3 months post-VEGF induction ('VEGF on') and 3 months after VEGF de-induction ('VEGF on>off') (Fig. 9*E*). While there was no difference between control and VEGF groups at baseline, VEGF-induced DG damage led to learning/memory impairment, reflected by more erroneous attempts before finding the platform. Following regeneration, impaired learning/memory was fully rectified, equalizing the performance of most treated mice to that of untreated littermates (Fig. 9*F*). The 5-day training progress for each one of the time points is presented in Fig. 9*G*. These results suggest that newly-born neurons produced during the repair phase may be functional, at least with respect to spatial learning and memory.

Regenerative potential of the DG is lost in old mice

Considering that hippocampal neurogenesis in rodents precipitously declines with age reaching a negligible level by the age of 9-12 months (Kuhn et al., 1996; Ben Abdallah et al., 2010; Encinas et al., 2011; Licht et al., 2016), it was of interest to determine whether regenerative potential also declines with age. To this end, VEGF induction and subsequent de-induction (for a period of 3 months each) were delayed such that the onset of VEGF induction was postponed to the age of 6 or 12 months (implying that regeneration was examined in 12 and 18 month-old mice, respectively, instead of in 8 month-old mice, as before (Fig. 10*A*)). It was first required l to ensure that a comparable DG injury is also elicited at older ages, i.e., that VEGF inducibility and responsiveness are not blunted with age. Preparatory experiments

JNeurosci Accepted Manuscript

showed that, at least with respect to the angiogenic response of VEGF, the aged (18m) hippocampus is as responsive as the young hippocampus (Fig. 10*B*). More directly, evaluation of the DG damage inflicted by VEGF exposure revealed a comparable decrease in DG cellularity and size in young and old mice (Fig. 10*B-F*). Twelve-month-old mice were still capable of mounting an efficient repair, evidenced by restoration of DG cellularity, size, and presence of the MF axonal layer in the majority of animals (but not all) (Fig. 10*B,E,F*). In contrast, 18 month-old mice appeared to have completely lost their regenerative capacity evidenced by a dramatically-reduced production of both DCX+ neuroblasts and NeuN+ neurons (Fig. 10*C,D*) and undetectable ZnT3+ MF (Fig. 10*B,E*). Cognitive decline and restoration could not be measured in this group of animals measured in this age group due to their deteriorated physical state precluding RAWM testing. These findings thus indicate that, in parallel to the age-related decay of DG neurogenesis, there is also a progressive loss in DG repair capability.

Discussion

The functional significance of adult hippocampal neurogenesis has been the subject for intensive research in the last three decades, with most studies attributing to added hippocampal neurons a role in learning and memory enhancement, depression and social behavior (Lee and Agoston, 2010; Marin-Burgin and Schinder, 2012; Toda and Gage, 2017). Little is known, however, whether the capacity of neuron production during adult life also serves the purpose of post-injury regeneration (Peng and Bonaguidi, 2018). The proposition of adult neurogenesis designated for regeneration was addressed through inflicting substantial DG-restricted damage using two unrelated methods and monitoring subsequent DG regeneration. Importantly, in the two model systems used, namely DT-aided GC ablation and

JNeurosci Accepted Manuscript

massive GC loss following sustained overexpression of ectopic VEGF, DG cellularity was dramatically reduced while NSCs were fully spared.

An intrinsic mechanism to cope with neuronal damage is of particular significance in the case of the DG given its exceptional vulnerability to many insults such as virus-induced encephalitis (Wu et al., 2013), exposure to chemicals (Bruccoleri et al., 1998; Choi et al., 2014; Choi et al., 2017) adrenalectomy/adrenal insufficiency (Spanswick et al., 2007; Spanswick et al., 2011; Izumida et al., 2017) Alzheimer's disease and frontotemporal lobe degeneration (Small et al., 2011; Armstrong et al., 2012; Adler et al., 2018). Our study adds yet another example for a selective DG vulnerability, namely, selective apoptosis of DG neurons following prolonged exposure to ectopic VEGF (a situation that can be physiologically relevant in the case of CNS tumors).

Could it be then that the DG neurogenic system serves as a backup system for homeostatic maintenance for this vulnerable organ? This would provide an additional rationale for the continued presence of NSCs in this specific locale. Notably, in comparison with the situation in mice where NSC-driven neurogenesis subsides with age, some findings show evidence for remaining neurogenesis in the adult human DG (Eriksson et al., 1998; Spalding et al., 2013; Boldrini et al., 2018), giving the option for a repair in old age.

Currently, we do not know why prolonged exposure to ectopic VEGF leads to hippocampal injury and, particularly, why the damage is restricted to DG GCs. Possible mechanisms of VEGF-induced neurotoxicity to be considered include: 1) Hyper-excitability and resultant glutamate toxicity due to increased LTP response, previously shown by us to be enhanced by VEGF in a reversible manner (Licht et al., 2011), a possibility also compatible with findings that NMDA receptor modulations in the hippocampus were shown to induce DG-specific degeneration while sparing the CA1 (Watanabe et al., 2016). 2) DG-specific damage could, in principle, be attributed to detrimental effects of ectopic neurogenesis (Cho et al., 2015). This possibility is, however, less likely considering that VEGF induces GCs death in aged mice

JNeurosci Accepted Manuscript

(where neurogenesis is negligible) 3) DG selectivity of VEGF-induced damage might also be related to VEGF-induced microglia activation which we found to be specific to the DG and precedes angiogenesis (Kreisel et al., 2018). Other possible explanations linked to the experimental tet system used were tested and precluded (Fig. 5). Regardless of the mechanism(s) underlying VEGF-induced neurotoxicity, both the magnitude of damage and its DG-restricted nature have provided us with a suitable platform for monitoring regeneration. Attesting for the remarkable regenerative potential of the DG was a significant restoration of DG cellularity (although not always achieving full recovery), proper rewiring of regenerated neurons and re-acquisition of lost spatial memory. The latter, however, was only demonstrated in the model of VEGF-induced DG injury, because in the DTR^{pomc} model, injured mice were still performing as well as untreated mice.

How the damage is sensed and the nature of factors triggering DG regeneration remains to be examined. Intriguingly, DG neurogenesis can be elicited not only in response to local signals but also in response to remote signals evidenced by a neurogenic response in the non-injured contralateral DG and even upon injury of other brain regions such as following a traumatic brain injury or cortical stroke (Jin et al., 2001; Zepeda et al., 2013; Wang et al., 2015). Interestingly, in our regeneration models, the addition of newborn neurons fully replaced lost GCs but the regenerated DG did not exceed its normal cellularity suggesting that a size control mechanism may exist.

The study shows that DG regeneration is solely driven by resident NSCs, thus anticipating (and indeed shown) that age-related NSC exhaustion will be reflected in age-related loss of regenerative potential. The ability to promote marked regeneration of DG morphology and functions by intrinsic stem cells is unique particularly when considering that SVZ-born NSCs, while capable of homing to remote injured brain areas (Nakatomi et al., 2002; Zhang et al., 2004; Grade et al., 2013) do not properly integrate and contribute to functional repair (Gould and Tanapat, 1997; Grade et al., 2013; Inta and Gass, 2015; Madathil and Saatman, 2015). One

JNeurosci Accepted Manuscript

notable difference in this regard is that, in the case of the hippocampus, newborn neurons remain in the boundaries of the DG and their integration in the existing network takes place within their natural microenvironment.

Demonstrating selective DG vulnerability and the ability of DG NSCs to promote repair highlights the regenerative designation of DG neurogenesis in the same line with its roles in learning and memory and gives an explanation for its presence particularly in this unique brain compartment.

References

Adler DH et al. (2018) Characterizing the human hippocampus in aging and Alzheimer's disease using a computational atlas derived from ex vivo MRI and histology. Proc Natl Acad Sci U S A 115:4252-4257.

Ahn S, Joyner AL (2004) Dynamic changes in the response of cells to positive hedgehog signaling during mouse limb patterning. Cell 118:505-516.

Aimone JB, Deng W, Gage FH (2011) Resolving new memories: a critical look at the dentate gyrus, adult neurogenesis, and pattern separation. Neuron 70:589-596.

Alamed J, Wilcock DM, Diamond DM, Gordon MN, Morgan D (2006) Two-day radial-arm water maze learning and memory task; robust resolution of amyloid-related memory deficits in transgenic mice. Nat Protoc 1:1671-1679.

Armstrong RA, Carter D, Cairns NJ (2012) A quantitative study of the neuropathology of 32 sporadic and familial cases of frontotemporal lobar degeneration with TDP-43 proteinopathy (FTLD-TDP). Neuropathol Appl Neurobiol 38:25-38.

Beard C, Hochedlinger K, Plath K, Wutz A, Jaenisch R (2006) Efficient method to generate single-copy transgenic mice by site-specific integration in embryonic stem cells. Genesis 44:23-28.

Ben Abdallah NMB, Slomianka L, Vyssotski AL, Lipp HP (2010) Early age-related changes in adult hippocampal neurogenesis in C57 mice. Neurobiol Aging 31:151-161.

Boldrini M, Fulmore CA, Tartt AN, Simeon LR, Pavlova I, Poposka V, Rosoklija GB, Stankov A, Arango V, Dwork AJ, Hen R, Mann JJ (2018) Human Hippocampal Neurogenesis Persists throughout Aging. Cell Stem Cell 22:589-599 e585.

Bruccoleri A, Brown H, Harry GJ (1998) Cellular localization and temporal elevation of tumor necrosis factor-alpha, interleukin-1 alpha, and transforming growth factor-beta 1 mRNA in hippocampal injury response induced by trimethyltin. J Neurochem 71:1577-1587.

Cho KO, Lybrand ZR, Ito N, Brulet R, Tafacory F, Zhang L, Good L, Ure K, Kernie SG, Birnbaum SG, Scharfman HE, Eisch AJ, Hsieh J (2015) Aberrant hippocampal neurogenesis contributes to epilepsy and associated cognitive decline. Nat Commun 6:6606.

Choi BY, Hong DK, Suh SW (2017) ZnT3 Gene Deletion Reduces Colchicine-Induced Dentate Granule Cell Degeneration. Int J Mol Sci 18.

JNeurosci Accepted Manuscript

Choi BY, Lee BE, Kim JH, Kim HJ, Sohn M, Song HK, Chung TN, Suh SW (2014) Colchicine induced intraneuronal free zinc accumulation and dentate granule cell degeneration. Metallomics 6:1513-1520.

Collins M, Riascos D, Kovalik T, An J, Krupa K, Hood BL, Conrads TP, Renton AE, Traynor BJ, Bowser R (2012) The RNA-binding motif 45 (RBM45) protein accumulates in inclusion bodies in amyotrophic lateral sclerosis (ALS) and frontotemporal lobar degeneration with TDP-43 inclusions (FTLD-TDP) patients. Acta Neuropathol 124:717-732.

Encinas JM, Michurina TV, Peunova N, Park JH, Tordo J, Peterson DA, Fishell G, Koulakov A, Enikolopov G (2011) Division-coupled astrocytic differentiation and age-related depletion of neural stem cells in the adult hippocampus. Cell Stem Cell 8:566-579.

Eriksson PS, Perfilieva E, Bjork-Eriksson T, Alborn AM, Nordborg C, Peterson DA, Gage FH (1998) Neurogenesis in the adult human hippocampus. Nat Med 4:1313-1317.

Fujisaki K, Tsuruya K, Yamato M, Toyonaga J, Noguchi H, Nakano T, Taniguchi M, Tokumoto M, Hirakata H, Kitazono T (2014) Cerebral oxidative stress induces spatial working memory dysfunction in uremic mice: neuroprotective effect of tempol. Nephrol Dial Transplant 29:529-538.

Gould E, Tanapat P (1997) Lesion-induced proliferation of neuronal progenitors in the dentate gyrus of the adult rat. Neuroscience 80:427-436.

Grade S, Weng YC, Snapyan M, Kriz J, Malva JO, Saghatelyan A (2013) Brain-derived neurotrophic factor promotes vasculature-associated migration of neuronal precursors toward the ischemic striatum. PLoS One 8:e55039.

Gray WP, Sundstrom LE (1998) Kainic acid increases the proliferation of granule cell progenitors in the dentate gyrus of the adult rat. Brain Res 790:52-59.

Han HJ, Allen CC, Buchovecky CM, Yetman MJ, Born HA, Marin MA, Rodgers SP, Song BJ, Lu HC, Justice MJ, Probst FJ, Jankowsky JL (2012) Strain background influences neurotoxicity and behavioral abnormalities in mice expressing the tetracycline transactivator. J Neurosci 32:10574-10586.

Hattiangady B, Rao MS, Shetty AK (2004) Chronic temporal lobe epilepsy is associated with severely declined dentate neurogenesis in the adult hippocampus. Neurobiol Dis 17:473-490.

Heinemann U, Beck H, Dreier JP, Ficker E, Stabel J, Zhang CL (1992) The dentate gyrus as a regulated gate for the propagation of epileptiform activity. Epilepsy Res Suppl 7:273-280.

Houser CR (1992) Morphological changes in the dentate gyrus in human temporal lobe epilepsy. Epilepsy Res Suppl 7:223-234.

Inta D, Gass P (2015) Is forebrain neurogenesis a potential repair mechanism after stroke? J Cereb Blood Flow Metab 35:1220-1221.

Izumida H, Takagi H, Fujisawa H, Iwata N, Nakashima K, Takeuchi S, Iwama S, Namba T, Komatu Y, Kaibuchi K, Oiso Y, Arima H, Sugimura Y (2017) NMDA receptor antagonist prevents cell death in the hippocampal dentate gyrus induced by hyponatremia accompanying adrenal insufficiency in rats. Exp Neurol 287:65-74.

Jessberger S, Zhao C, Toni N, Clemenson GD, Jr., Li Y, Gage FH (2007) Seizure-associated, aberrant neurogenesis in adult rats characterized with retrovirus-mediated cell labeling. J Neurosci 27:9400-9407.

Jin K, Minami M, Lan JQ, Mao XO, Batteur S, Simon RP, Greenberg DA (2001) Neurogenesis in dentate subgranular zone and rostral subventricular zone after focal cerebral ischemia in the rat. Proc Natl Acad Sci U S A 98:4710-4715.

Jin KL, Mao XO, Greenberg DA (2000) Vascular endothelial growth factor: Direct neuroprotective effect in in vitro ischemia. P Natl Acad Sci USA 97:10242-10247.

Kivela R, Hemanthakumar KA, Vaparanta K, Robciuc M, Izumiya Y, Kidoya H, Takakura N, Peng X, Sawyer DB, Elenius K, Walsh K, Alitalo K (2019) Endothelial Cells Regulate

JNeurosci Accepted Manuscript

Physiological Cardiomyocyte Growth via VEGFR2 -Mediated Paracrine Signaling. Circulation.

Kovacs GG et al. (2013) Neuropathology of the hippocampus in FTLD-Tau with Pick bodies: a study of the BrainNet Europe Consortium. Neuropathol Appl Neurobiol 39:166-178.

Kreisel T, Wolf B, Keshet E, Licht T (2018) Unique role for dentate gyrus microglia in neuroblast survival and in VEGF-induced activation. Glia.

Krook-Magnuson E, Armstrong C, Bui A, Lew S, Oijala M, Soltesz I (2015) In vivo evaluation of the dentate gate theory in epilepsy. J Physiol.

Kuhn HG, DickinsonAnson H, Gage FH (1996) Neurogenesis in the dentate gyrus of the adult rat: Age-related decrease of neuronal progenitor proliferation. Journal of Neuroscience 16:2027-2033.

Kukreja L, Shahidehpour R, Kim G, Keegan J, Sadleir KR, Russell T, Csernansky J, Mesulam M, Vassar RJ, Wang L, Dong H, Geula C (2018) Differential Neurotoxicity Related to Tetracycline Transactivator and TDP-43 Expression in Conditional TDP-43 Mouse Model of Frontotemporal Lobar Degeneration. J Neurosci 38:6045-6062.

Lee C, Agoston DV (2010) Vascular endothelial growth factor is involved in mediating increased de novo hippocampal neurogenesis in response to traumatic brain injury. J Neurotrauma 27:541-553.

Licht T, Keshet E (2015) The vascular niche in adult neurogenesis. Mech Dev 138 Pt 1:56-62.

Licht T, Eavri R, Goshen I, Shlomai Y, Mizrahi A, Keshet E (2010) VEGF is required for dendritogenesis of newly born olfactory bulb interneurons. Development 137:261-271.

Licht T, Goshen I, Avital A, Kreisel T, Zubedat S, Eavri R, Segal M, Yirmiya R, Keshet E (2011) Reversible modulations of neuronal plasticity by VEGF. Proc Natl Acad Sci U S A 108:5081-5086.

Licht T, Rothe G, Kreisel T, Wolf B, Benny O, Rooney AG, Ffrench-Constant C, Enikolopov G, Keshet E (2016) VEGF preconditioning leads to stem cell remodeling and attenuates age-related decay of adult hippocampal neurogenesis. Proc Natl Acad Sci U S A 113:E7828-E7836.

Lu J, Manaenko A, Hu Q (2017) Targeting Adult Neurogenesis for Poststroke Therapy. Stem Cells Int 2017:5868632.

Madathil SK, Saatman KE (2015) IGF-1/IGF-R Signaling in Traumatic Brain Injury: Impact on Cell Survival, Neurogenesis, and Behavioral Outcome.

Maehlen J, Torvik A (1990) Necrosis of granule cells of hippocampus in adrenocortical failure. Acta Neuropathol 80:85-87.

Marin-Burgin A, Schinder AF (2012) Requirement of adult-born neurons for hippocampus-dependent learning. Behav Brain Res 227:391-399.

Mayford M, Bach ME, Huang YY, Wang L, Hawkins RD, Kandel ER (1996) Control of memory formation through regulated expression of a CaMKII transgene. Science 274:1678-1683.

McHugh TJ, Jones MW, Quinn JJ, Balthasar N, Coppari R, Elmquist JK, Lowell BB, Fanselow MS, Wilson MA, Tonegawa S (2007) Dentate gyrus NMDA receptors mediate rapid pattern separation in the hippocampal network. Science 317:94-99.

Melander A et al. (1999) 35th Annual Meeting of the European Association for the Study of Diabetes : Brussels, Belgium, 28 September-2 October 1999. Diabetologia 42:A1-A330.

Melnikova T, Park D, Becker L, Lee D, Cho E, Sayyida N, Tian J, Bandeen-Roche K, Borchelt DR, Savonenko AV (2016) Sex-related dimorphism in dentate gyrus atrophy and behavioral phenotypes in an inducible tTa:APPsi transgenic model of Alzheimer's disease. Neurobiol Dis 96:171-185.

JNeurosci Accepted Manuscript

Mignone JL, Kukekov V, Chiang AS, Steindler D, Enikolopov G (2004) Neural stem and progenitor cells in nestin-GFP transgenic mice. Journal of Comparative Neurology 469:311-324.

Moss J, Gebara E, Bushong EA, Sanchez-Pascual I, O'Laoi R, El M'Ghari I, Kocher-Braissant J, Ellisman MH, Toni N (2016) Fine processes of Nestin-GFP-positive radial glia-like stem cells in the adult dentate gyrus ensheathe local synapses and vasculature. Proc Natl Acad Sci U S A 113:E2536-2545.

Myczek K, Yeung ST, Castello N, Baglietto-Vargas D, LaFerla FM (2014) Hippocampal adaptive response following extensive neuronal loss in an inducible transgenic mouse model. PLoS One 9:e106009.

Nakatomi H, Kuriu T, Okabe S, Yamamoto S, Hatano O, Kawahara N, Tamura A, Kirino T, Nakafuku M (2002) Regeneration of hippocampal pyramidal neurons after ischemic brain injury by recruitment of endogenous neural progenitors. Cell 110:429-441.

Oosthuyse B et al. (2001) Deletion of the hypoxia-response element in the vascular endothelial growth factor promoter causes motor neuron degeneration. Nature Genetics 28:131-138.

Palmiter RD, Cole TB, Quaife CJ, Findley SD (1996) ZnT-3, a putative transporter of zinc into synaptic vesicles. Proc Natl Acad Sci U S A 93:14934-14939.

Peng L, Bonaguidi MA (2018) Function and Dysfunction of Adult Hippocampal Neurogenesis in Regeneration and Disease. Am J Pathol 188:23-28.

Sierra A, Martin-Suarez S, Valcarcel-Martin R, Pascual-Brazo J, Aelvoet SA, Abiega O, Deudero JJ, Brewster AL, Bernales I, Anderson AE, Baekelandt V, Maletic-Savatic M, Encinas JM (2015) Neuronal hyperactivity accelerates depletion of neural stem cells and impairs hippocampal neurogenesis. Cell Stem Cell 16:488-503.

Sirerol-Piquer M, Gomez-Ramos P, Hernandez F, Perez M, Moran MA, Fuster-Matanzo A, Lucas JJ, Avila J, Garcia-Verdugo JM (2011) GSK3beta overexpression induces neuronal death and a depletion of the neurogenic niches in the dentate gyrus. Hippocampus 21:910-922.

Small SA, Schobel SA, Buxton RB, Witter MP, Barnes CA (2011) A pathophysiological framework of hippocampal dysfunction in ageing and disease. Nat Rev Neurosci 12:585-601.

Spalding KL, Bergmann O, Alkass K, Bernard S, Salehpour M, Huttner HB, Bostrom E, Westerlund I, Vial C, Buchholz BA, Possnert G, Mash DC, Druid H, Frisen J (2013) Dynamics of hippocampal neurogenesis in adult humans. Cell 153:1219-1227.

Spanswick SC, Lehmann H, Sutherland RJ (2011) A novel animal model of hippocampal cognitive deficits, slow neurodegeneration, and neuroregeneration. J Biomed Biotechnol 2011:527201.

Spanswick SC, Epp JR, Keith JR, Sutherland RJ (2007) Adrenalectomy-induced granule cell degeneration in the hippocampus causes spatial memory deficits that are not reversed by chronic treatment with corticosterone or fluoxetine. Hippocampus 17:137-146.

Steward O (1994) Electroconvulsive seizures upregulate astroglial gene expression selectively in the dentate gyrus. Brain Res Mol Brain Res 25:217-224.

Takeda A, Tamano H (2018) Is Vulnerability of the Dentate Gyrus to Aging and Amyloid-beta1-42 Neurotoxicity Linked with Modified Extracellular Zn(2+) Dynamics? Biol Pharm Bull 41:995-1000.

Toda T, Gage FH (2017) Review: adult neurogenesis contributes to hippocampal plasticity. Cell and Tissue Research.

Toda T, Parylak SL, Linker SB, Gage FH (2018) The role of adult hippocampal neurogenesis in brain health and disease. Mol Psychiatry.

JNeurosci Accepted Manuscript

Tu DG, Chang YL, Chou CH, Lin YL, Chiang CC, Chang YY, Chen YC (2018) Preventive effects of taurine against d-galactose-induced cognitive dysfunction and brain damage. Food Funct 9:124-133.

van Praag H, Schinder AF, Christie BR, Toni N, Palmer TD, Gage FH (2002) Functional neurogenesis in the adult hippocampus. Nature 415:1030-1034.

Wang F, Fangfang Z, Guo X, Chen W, Yao W, Liu H, Lyu C, Zhang Y, Fan C (2018) Effects of volatile organic compounds and carbon monoxide mixtures on learning and memory, oxidative stress, and monoamine neurotransmitters in the brains of mice. Toxicol Ind Health 34:178-187.

Wang X, Gao X, Michalski S, Zhao S, Chen J (2015) Traumatic Brain Injury Severity Affects Neurogenesis in Adult Mouse Hippocampus. J Neurotrauma.

Watanabe Y, Muller MK, von Engelhardt J, Sprengel R, Seeburg PH, Monyer H (2016) Age-Dependent Degeneration of Mature Dentate Gyrus Granule Cells Following NMDA Receptor Ablation. Front Mol Neurosci 8.

Wu YJ, Schulz H, Lin CC, Saar K, Patone G, Fischer H, Hubner N, Heimrich B, Schwemmle M (2013) Borna disease virus-induced neuronal degeneration dependent on host genetic background and prevented by soluble factors. P Natl Acad Sci USA 110:1899-1904.

Yamasaki TR, Blurton-Jones M, Morrissette DA, Kitazawa M, Oddo S, LaFerla FM (2007) Neural stem cells improve memory in an inducible mouse model of neuronal loss. J Neurosci 27:11925-11933.

Yu TS, Washington PM, Kernie SG (2016) Injury-Induced Neurogenesis: Mechanisms and Relevance. Neuroscientist 22:61-71.

Zepeda A, Aguilar-Arredondo A, Michel G, Ramos-Languren LE, Escobar ML, Arias C (2013) Functional recovery of the dentate gyrus after a focal lesion is accompanied by structural reorganization in the adult rat. Brain Struct Funct 218:437-453.

Zhang R, Zhang Z, Wang L, Wang Y, Gousev A, Zhang L, Ho KL, Morshead C, Chopp M (2004) Activated neural stem cells contribute to stroke-induced neurogenesis and neuroblast migration toward the infarct boundary in adult rats. J Cereb Blood Flow Metab 24:441-448.

Figure legends

Fig. 1.

Diphtheria toxin-mediated specific ablation of DG GCs. ***A***, Protocol for highlighting the pattern of cre-expressing cells in the POMC-Cre transgenic mouse line with the aid of Ai9 reporter mouse. ***B***, Pomc-Cre drives TdTomato reporter expression specifically in the DG (yellow arrows). Right: NSCs distinguished by their tree-like morphology and highlighted by GFP in the Nestin-GFP line do not co-localize with TdTomato (see arrows in z-projection planes). Scale

JNeurosci Accepted Manuscript

bars, 1mm (left and middle), 50µm (right). ***C***, Pomc-Cre does not drive expression of the TdTomato reporter in DCX^+ neuroblasts (arrows). Scale bar, 100µm. ***D,*** Experimental protocol for Cre-mediated cell ablation using iDTR mice for conditional expression of DTR (DTR^{pomc}). ***E***, DT (5ng) was injected to the left hippocampus of DTR^{pomc} mice and brains were retrieved 5 days thereafter. Cleaved-caspase 3 immunostaining illustrates a DG-restricted injury (left) and Iba1 immunostaining highlights microglia clustering in the injured GCL of the DG (right). i-ipsilateral. c-contralateral. Scale bar, 1mm (left), 200µm (right). ***F-G,*** DT (3ng) was injected bilaterally to the hippocampus of control (iDTR monotransgenic) or DTR^{pomc} mice and brains were retrieved 20 or 90 days later. A substantial loss of GCs in DTR^{pomc} mice is indicated at 20 dpi by NeuN immunostaining highlighting GC cell bodies (***F***) and by ZnT3 immunostaining highlighting their MF axons (***G***.) Near-complete recovery is indicated at 90 dpi. Scale bar, 100µm. ***H,*** DG height (yellow bar), GCL thickness (white bar) and thickness of the MF layer (red bar) used as quantifiable parameters of DG repair (shown in control DG). Scale bar, 100µm. ***I***, Quantification of DG regeneration comparing non-injured, injured (at 20 dpi) and repaired (at 90 dpi) hippocampi.

For statistical details see Table 1.

Fig. 2.

Neurogenesis-driven DG regeneration in DTR^{pomc} mice. ***A,*** DT (3ng) was injected bilaterally to the hippocampus of control iDTR mice or to DTR^{pomc} mice. Mice also harbored a Nestin-GFP transgene to highlight NSCs. CldU (100mg/kg 3 i.p injections every 12h) was injected at 15-16 dpi and brains were retrieved at 20dpi. Relevant for ***B-F***. ***B,*** RGL-type NSCs highlighted with Nestin-GFP (top) together with $NeuN^+$ mature neurons and $CD31^+$ blood vessels at higher magnification (Melander et al.). Note the loss of NSCs apical processes (arrows) and massive mature neurons deficit in DTR^{pomc} mice. Scale bar, 100µm. Right: quantification for NSCs

JNeurosci Accepted Manuscript

density revealed no significant change in their numbers. ***C,*** CldU immunostaining highlights intensive GCL-specific cell labeling in DTR^{pomc} DG. Scale bar, 200µm. ***D,*** CldU immunostaining together with the visualization of GFP^+ cells highlights active NSCs (RGL (R) and descendants). Right: A particular example of a 'clone' composed of an RGL (R) and assumed daughter progenitors (labeled 1-6) in DTR^{pomc}. Scale bar, 10µm. ***E,*** CldU and DCX co-staining highlights 4-5 days-old early neuroblasts. Right: A representative image in an orthogonal plane showing co-localization of DCX and CldU. ***F,*** Quantification of ***D-E***. ***G***, To allow sufficient time for regeneration, brains were retrieved for analysis 90 days post-injection (90 dpi). ***H***, Measurements of differentiation to newly-added neurons by 90 dpi were enumerated through CldU injection 1 month earlier (the time required for newborn neuroblasts to mature) and scoring for double-positive $Cldu^+/NeuN^+$ cells in the GCL. Scale bar, 100µm. ***I,*** Brains of DTR^{pomc} mice retrieved at 90 dpi and stained for cleaved caspase 3 and for DTR (top) and for microglia (Melander et al.) indicate an ongoing DG toxicity 90 days from DT injection. Scale bar, 200µm.

For statistical details see Table 1.

Fig. 3.

Neurogenesis and DG injury induced by long term VEGF exposure. ***A***, Tetracycline-regulated transgenic system for VEGF expression in the brain. ***B,*** VEGF was induced ("on") in adult (2months) mice by tetracycline withdrawal and was kept in the 'on' mode for the indicated periods. Littermates harboring only the driver transgene served as controls. ***C,*** VEGF-induced neurogenesis reflected in an increased number of DCX^+ cells (neuroblasts and immature neurons) in the DG. Bottom: Quantification of DCX^+ cells in the DG in hippocampi removed at the indicated times post VEGF induction. Note that, on the contrary to natural neurogenic decline in control mice, an elevated neurogenic rate persists throughout the 7 months' period of continuous VEGF exposure. ***D***, NeuN staining (labeling mature neurons) Highlights dramatic

JNeurosci Accepted Manuscript

neuronal loss in the DG of prolonged VEGF-expressing animals. Scale bar, 100µm. Bottom: Average GCL area measured in NeuN-stained DG sections.

For statistical details see Table 1.

Fig. 4.

Global long term VEGF overexpression induces DG-specific injury**. *A,*** CamKIIα -tTA mouse was crossed to the Tet-GFP responder line to highlight which areas are affected by the transgenic system. GFP in coronal (left) and sagittal (middle) sections is mainly expressed in the hippocampus (Hip), the cerebral peduncles (cpd) and the striatum (STR) and to a lesser extent in the cortex (CTX) and olfactory bulb (OB). Note that within the hippocampus, GFP expression is stronger in the CA1 (right). Scale bar, 1mm. ***B,*** Adult (2months) CamKIIα-tTA tet-VEGF mice were subjected to VEGF induction for 4 months. VEGF-induced angiogenesis reflected in microvascular density (MVD) increase in both DG and CA1 regions of the hippocampus. Left: blood vessels highlighted by laminin immunostaining. Scale bar, 200µm. Note DG-selective degeneration in the 4m VEGF mouse. Right: MVD quantification in the respective hippocampal region showing equal angiogenic responsiveness to VEGF in both areas. ***C,*** The CA1 area of the same mice as in (**B**) was immunostained for CD31 and NeuN. Scale bar, 50 µm. Right: quantification. Note that the height of CA1 in VEGF animals is slightly larger than control animals, a potential reflection of extensive blood vessel formation. ***D,*** Low magnification images of the whole brain to highlight DG-selectivity of the detrimental response to VEGF. Immunostaining for cleaved-caspase 3 (CC3), Iba1 for microglia and GFAP for astrocytes is shown. The CA1 is indicated by white arrows, DG is indicated by yellow arrows. Scale bars, 1mm. ***E***, High magnification images of CC3, Iba1 and GFAP in control animals, 1m VEGF induction, 3m VEGF induction and following additional 3m of VEGF withdrawal (VEGF on>off). The CA1 is indicated by white arrows, the DG is indicated by yellow arrows. Note that similarly

JNeurosci Accepted Manuscript

to the DTR^{pomc} model, the majority of cleaved-caspase 3 is localized in the molecular layer (ML) of the DG. Scale bars, 200µm.

For statistical details see Table 1.

Fig. 5.

Precluding potential mechanisms for DG-specific damage in the CamkIIα-tTA;;tet-VEGF mouse model. ***A,*** To test for DG-specific changes in permeability following VEGF induction, Tritc-labeled 10kD dextran (tracer) was injected intracardially 2 minutes before sacrifice. Co-staining with CD31 for endothelial cells demonstrates that dextran labeling is limited to the endothelial lumen. ***B-D,*** CamkIIα-tTA mouse line-related toxicity. ***B,*** NeuN-stained hippocampal slices of six-months-old mice (from the same litter) are presented. The genotype of each animal is indicated above. Tetracycline was replaced by water at the age of 2 months in all mice. ***C,*** CamkIIα-tTA driver line was crossed to a tet-GFP responder line. Tetracycline was omitted from drinking water at the age of 2 months to 6 months. Note intact mossy fiber axon indicated by ZnT3 staining. Quantification of DG height and GCL thickness is presented. So significance was found. ***D,*** CamkIIα-tTA driver line was crossed to a tet-hsVEGFR1 line. This mouse line expresses inducible soluble human VEGF receptor 1 that serves as a "VEGF trap" (Licht et al., 2010). Tetracycline was replaced by water from embryonic day 14.5 to 6 months postnatally. ***E,*** Intrahippocampal injection of AAV encoding VEGF induces DG damage which is similar to transgenically-induced VEGF. DCX immunostaining is shown. Note the reduction in GCL thickness (yellow bars) and ectopic neurogenesis.

Scale bars, 200µm.

For statistical details see Table 1.

JNeurosci Accepted Manuscript

Fig. 6.

The injury to the DG following long term VEGF exposure is rectified upon VEGF de-induction. ***A***, Experimental protocol: 'off' group – monotransgenic littermates sacrificed at 5 months; 'on' group - VEGF induced at the age of 2 months and brains retrieved at 5 months; 'on>off' group - VEGF induced at 2 months, de-induced at 5 months and sacrificed at 8 months (on>off). ***B,*** NeuN-immunostained DG sections showing a marked neuronal deficit in 'VEGF on' mice and neuronal re-gain 3 months after VEGF de-induction. Scale bars: 200µm (top), 50µm (Melander et al.). ***C,*** ZnT3-stained sections highlighting MF axon of GCs. Scale bar, 100µm. ***D,*** Quantification of DG measurements as above indicative of neuronal cell loss and of neuronal re-gain (although not the reaching same values of control). ***E,*** Quantification of GCL area (using NeuN-stained sections) as in Fig. **3D**, with the addition of the 'on<off' group. Arrow indicates time of tetracycline supplementation for the on>off groups.

For statistical details see Table 1.

Fig. 7.

NSCs proliferation during DG degeneration and recovery. ***A,*** Nestin-GFP transgenic mice were crossed to the VEGF transgenic system. VEGF was induced for 3 months followed by de-induction of additional 3 months. IdU (100mg/kg) was applied I.P 1-2 days before brain retrieval. ***B,*** Slices were co-immunostained for GFP and for Laminin to highlight blood vessels. Scale bar, 200µm. Note contact points of NSCs' apical processes with blood vessels (arrows). ***C,*** GFP and IdU immunostaining (Scale bar, 20µm). ML- molecular layer. H – hilus. Note hilar projections of NSCs in 'VEGF on' animal (Arrows). ***D,*** The total numbers of GFP+ NSCs and the fraction of dividing NSCs (IdU+) are quantified. A significant increase in NSC proliferation in both on and on>off groups overrides expected NSC exhaustion.

For statistical details see Table 1.

JNeurosci Accepted Manuscript

Fig. 8.

Differentiation and maturation of DG newborn cells during degeneration and regeneration. ***A***, Schedules of VEGF induction and, in turn, de-induction relevant to ***B-D***. CldU was injected (3 IP injections of 100mg/kg every 8 hours) 3 weeks before brain retrieval to allow for sufficient time for newborn cell maturation. ***B***, Left: co-staining for CldU and NeuN highlighting neurons that have been born and differentiated during the preceding 3 weeks. Scale bar, 100µm. Right: quantification of $CldU^+/NeuN^+$ cell densities. Note a significant addition of $NeuN^+$ cells following VEGF de-induction but not when VEGF signaling was still ongoing. ***C,*** DCX and CD31 staining highlighting neuroblasts and blood vessels, respectively. Note ectopic DCX^+ cells in the hilus (inset 1) and in the molecular layer (inset 2). Scale bar, 100µm. Quantification of $CD31^+$ cells shows that blood vessels added by VEGF persists after its withdrawal (MVD, right) and likewise, quantification of total DCX^+ cell numbers shows that neuroblast production remains at approximately the same elevated levels after VEGF withdrawal. ***D,*** Co-staining for DCX and CldU to label late (3 weeks-old) neuroblasts, prior to completion of maturation. Quantification of late neuroblast density and percentage on right. ***E-H,*** Aberrant aspects of neurogenesis revealed by tracing Gli^+ NSC descendants. ***E***, Experimental scheme: Gli1-cre^{ERT2} and Ai9 reporter mice were bred to the VEGF system. ***F***, Animals which inherited all four transgenes were fed by Tamoxifen (8mg, 1/day oral administration for 3 days) Brains were retrieved for analysis according to the scheme. ***G,*** Representative images of $Gli1^+$ cells and their descendants with dendrite morphologies better seen in high magnification insets. Note lack of dendritic spines in "VEGF on" dendrites (iv) and their presence in the "VEGF on>off" (vi). Arrows indicate NSCs and adult-born GCs according to the legends in ***H***. ML- molecular layer. H-hilus. Scale bar, 100µm. ***H,*** Analysis for the percentage of cell types (NSCs and GCs) in each of the experimental protocols.

JNeurosci Accepted Manuscript

For statistical details see Table 1.

Fig. 9.

Regeneration of Perforant path connectivity and spatial memory. ***A,*** Experimental design for B-D. ***B,*** Acute coronal slices from 'VEGF on' and 'on>off' mice were stimulated at the afferent fibers of the Perforant path (S) and EPSP was recorded at the upper blade of the GCL (R). ***C***, Representative traces in control, 'on' and 'on>off' hippocampal slices. ***D,*** Peak EPSP amplitude at the stimulation of 16V was measured. ***E,*** Radial Arm Water Maze (RAWM) testing. A group of double-transgenic animals and their littermate controls was tested at three-time points: before VEGF induction, 3 months from inducing VEGF and after 3 additional months of de-induction. A significantly higher number of errors to find the platform is found only in the "VEGF on" group. ***F,*** Impaired learning in the VEGF-on group is reflected in more erroneous trials before finding the escape platform. 3 months after VEGF de-induction learning abilities are fully restored. ***G,*** The numbers of errors during the training period at every time point. For statistical details see Table 1.

Fig. 10.

The regenerative potential of the DG is lost in old age. ***A,*** Experimental protocol: VEGF was induced at the ages of 6 or 12 months, maintained for 3 months in the 'on' mode and then de-induced. Brains were retrieved for analysis either by the end of the induction period (for measuring incurred damage) or 3 months after de-induction (i.e., when mice are 12- and 18 months old, respectively) for measuring the extent of structural repair. ***B,*** Immunostaining for ZnT3 and CD31. Right: MVD quantification for 18 months old animals**.** Note that old mice

JNeurosci Accepted Manuscript

display angiogenic response to VEGF similarly to young mice. ***C,*** Immunostaining for DCX and NeuN**.** DCX cell density quantification is presented on the right. ***D***, CldU was injected 3 weeks before sacrifice and $CldU^+/NeuN^+$ cells were visualized (left images) and quantified (right). ***E,*** High power field of CA3 ZnT3 staining. MF thickness (quantified in right) was measured as in Fig. 1*H*. ***F***,***G*** NeuN staining (*C, D*) was used to measure GCL thickness (***F***) and DG height (***G***) as in Fig. 2*B*.

Scale bars, 100µm.

For statistical details see Table 1.

Table legends

Table 1.

Statistical analysis for all quantifications. The number of animals, statistical tests, statistical power and p-values are presented.

JNeurosci Accepted Manuscript

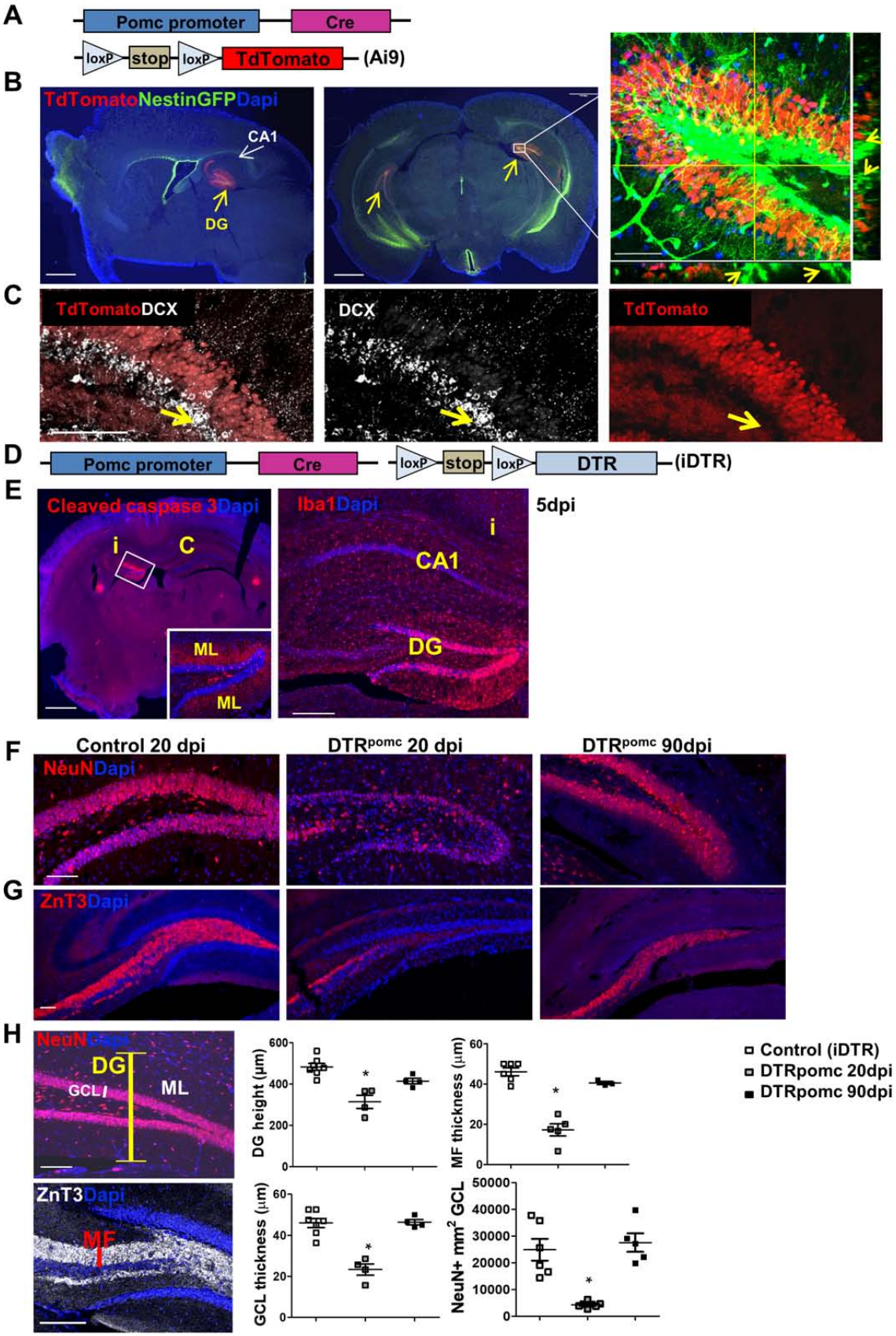

JNeurosci Accepted Manuscript

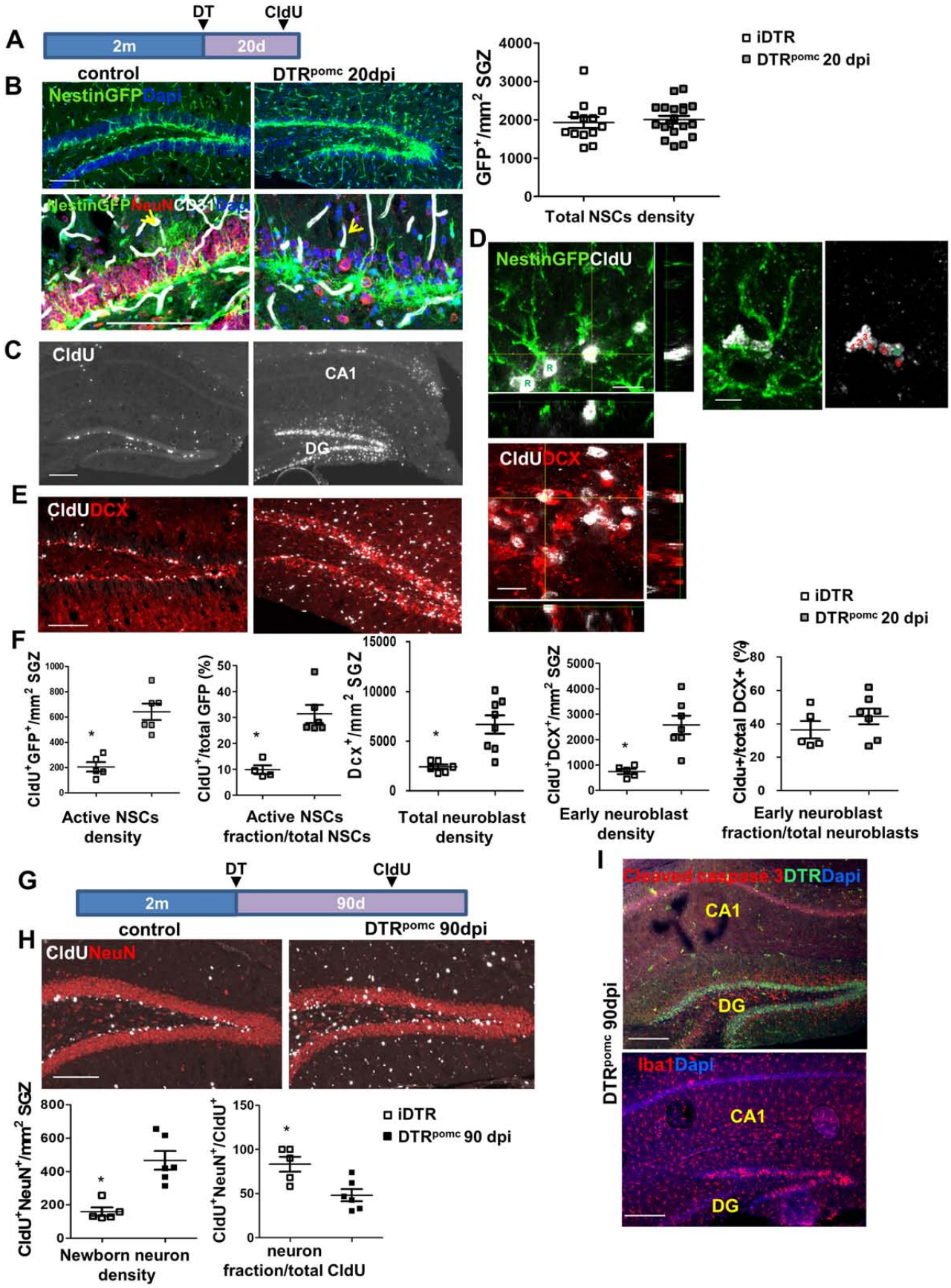

JNeurosci Accepted Manuscript

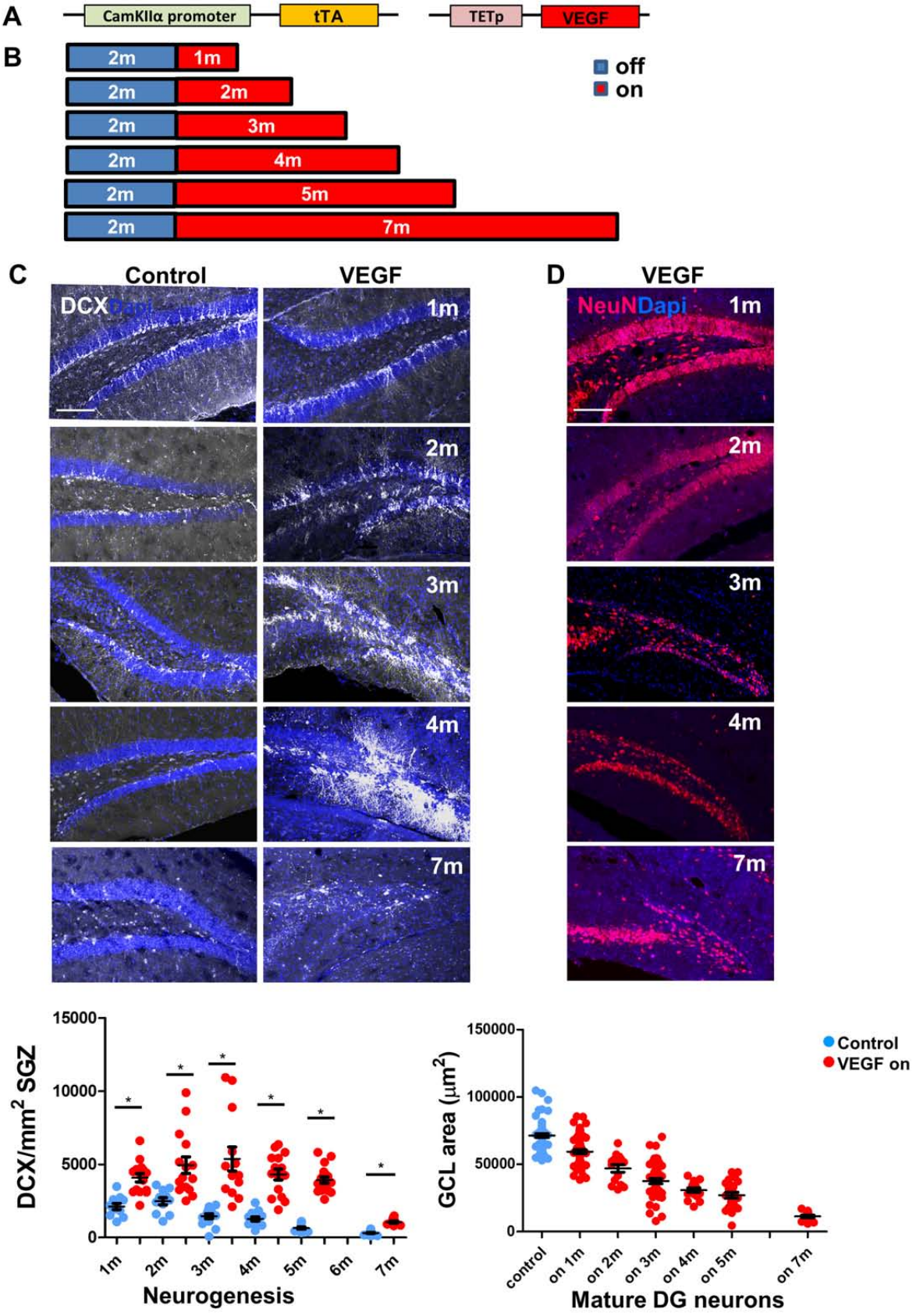

JNeurosci Accepted Manuscript

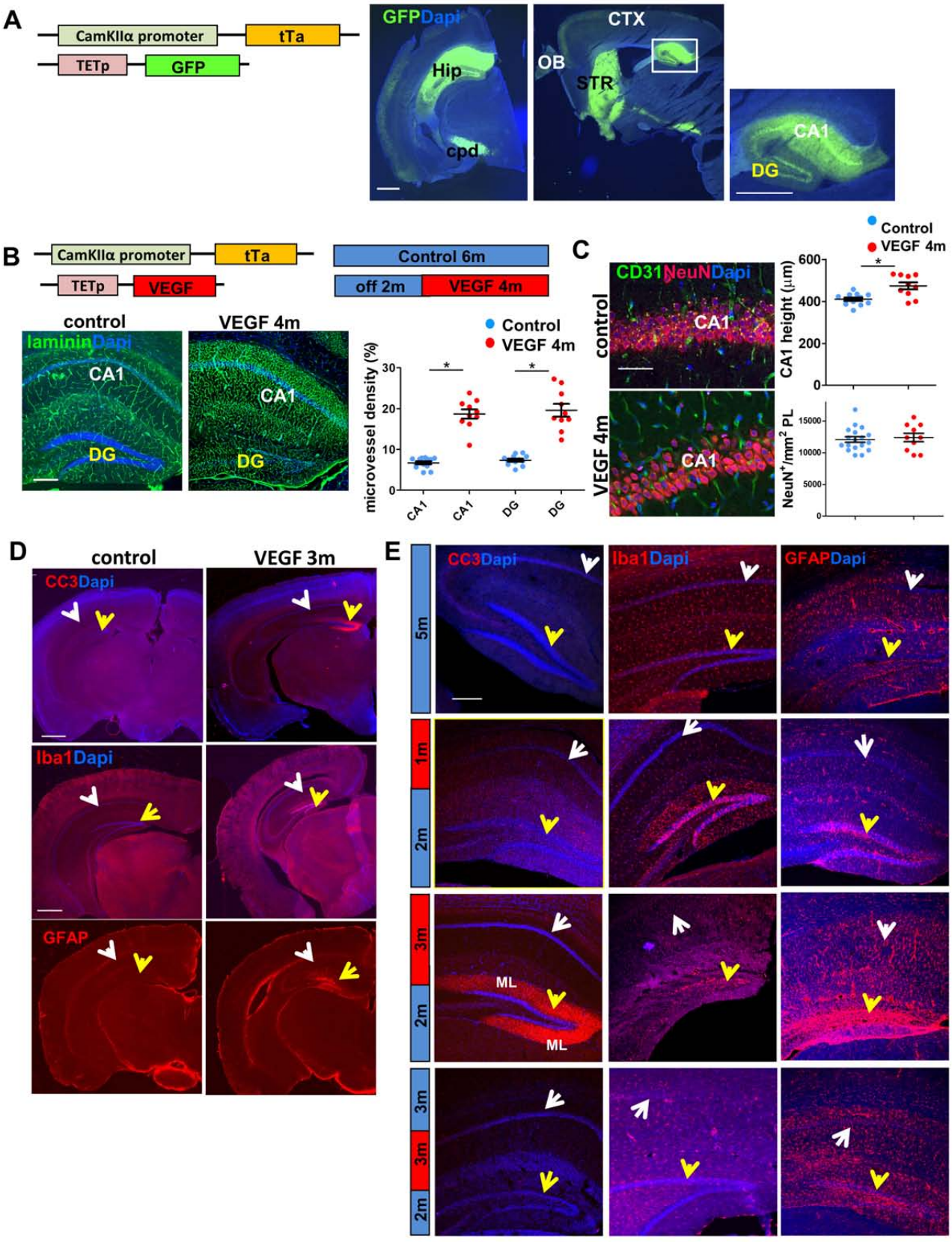

JNeurosci Accepted Manuscript

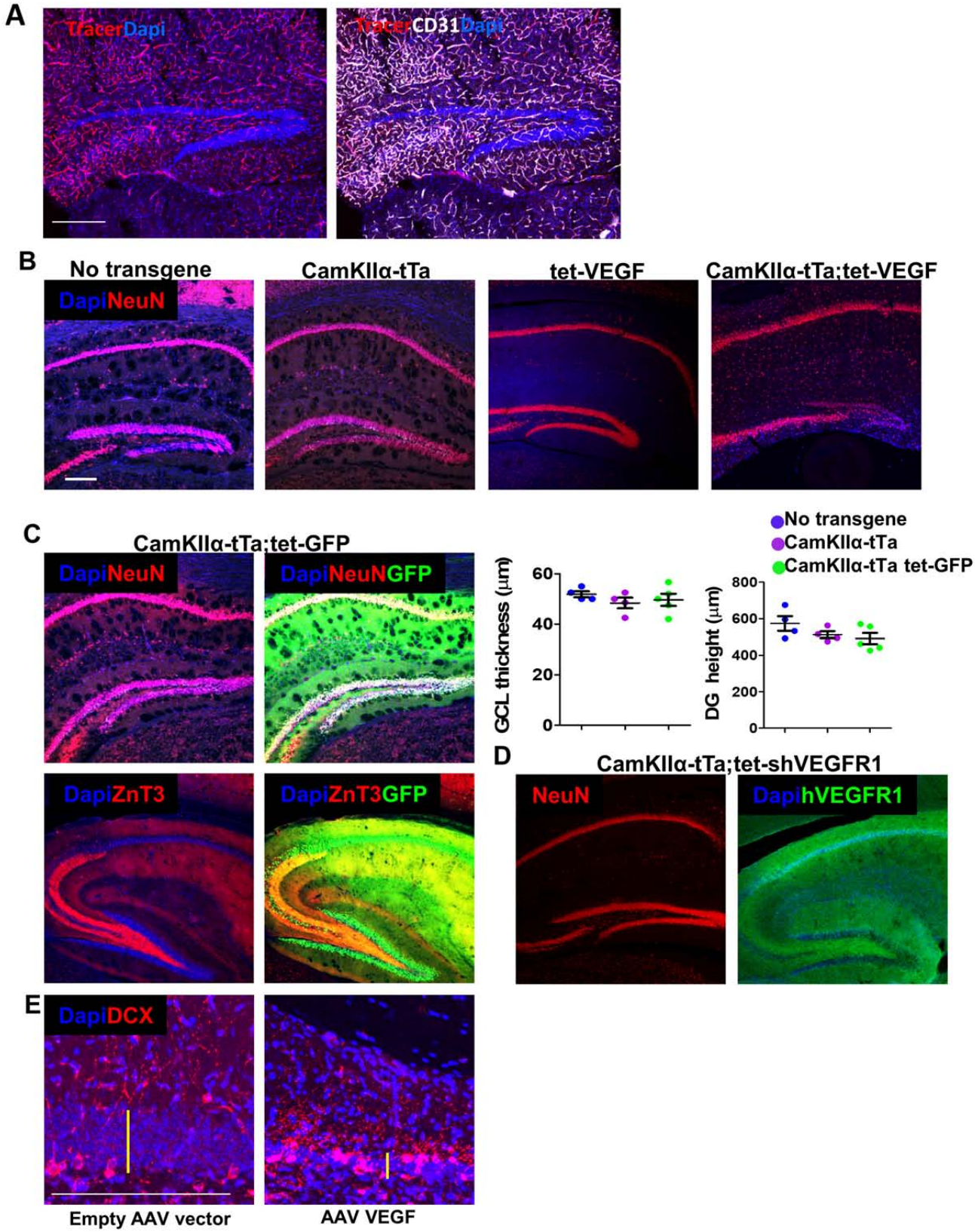

JNeurosci Accepted Manuscript

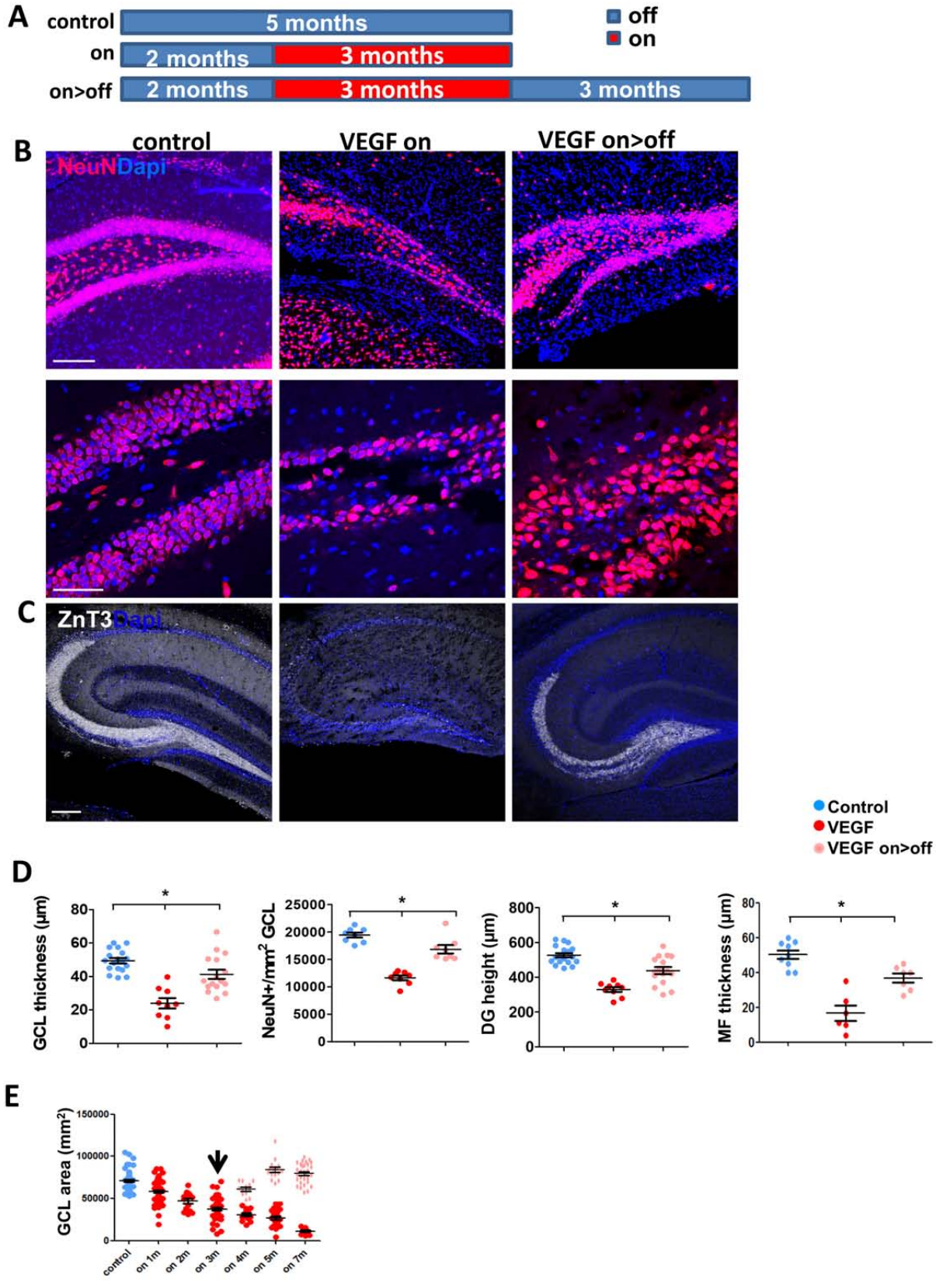

JNeurosci Accepted Manuscript

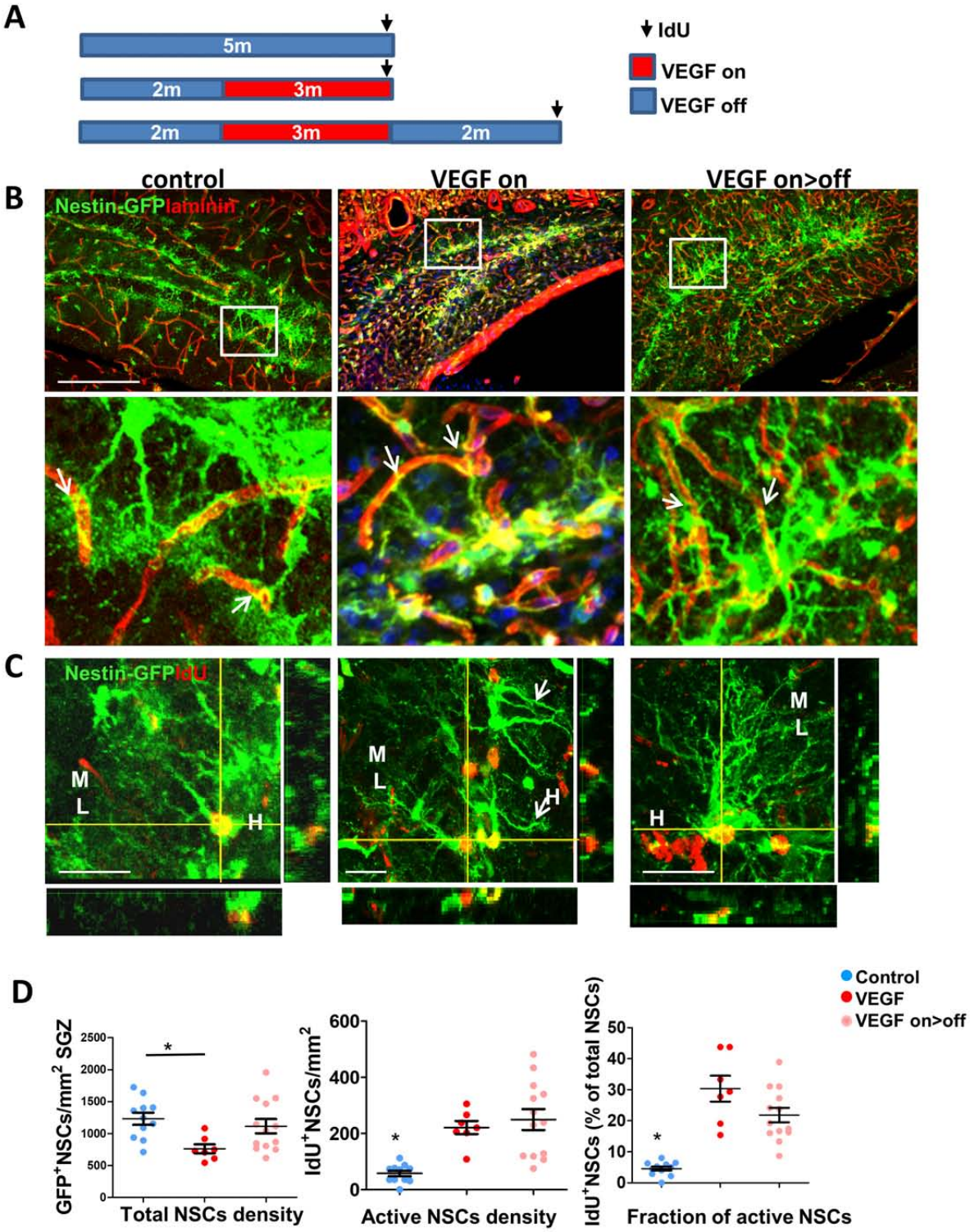

JNeurosci Accepted Manuscript

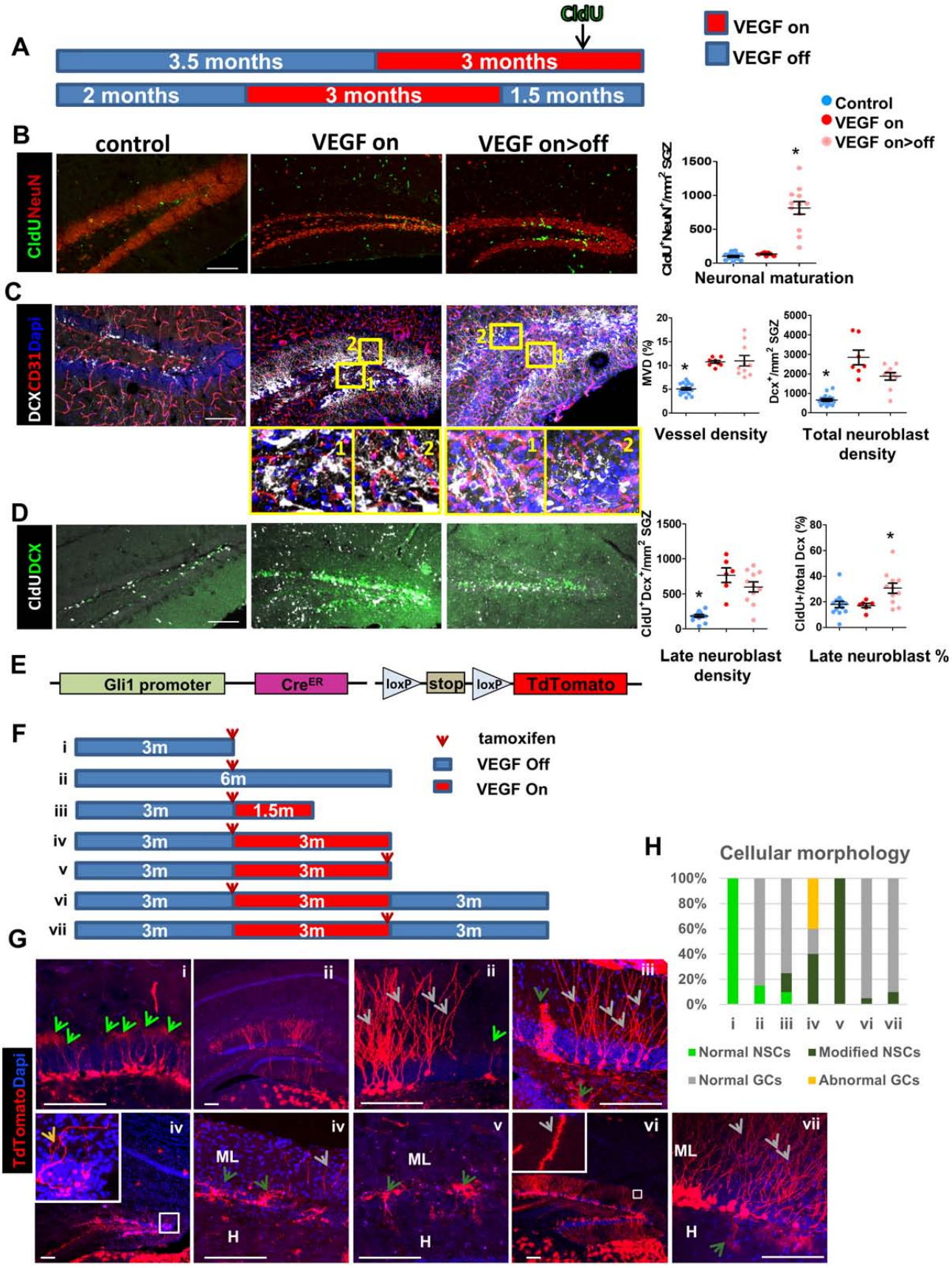

JNeurosci Accepted Manuscript

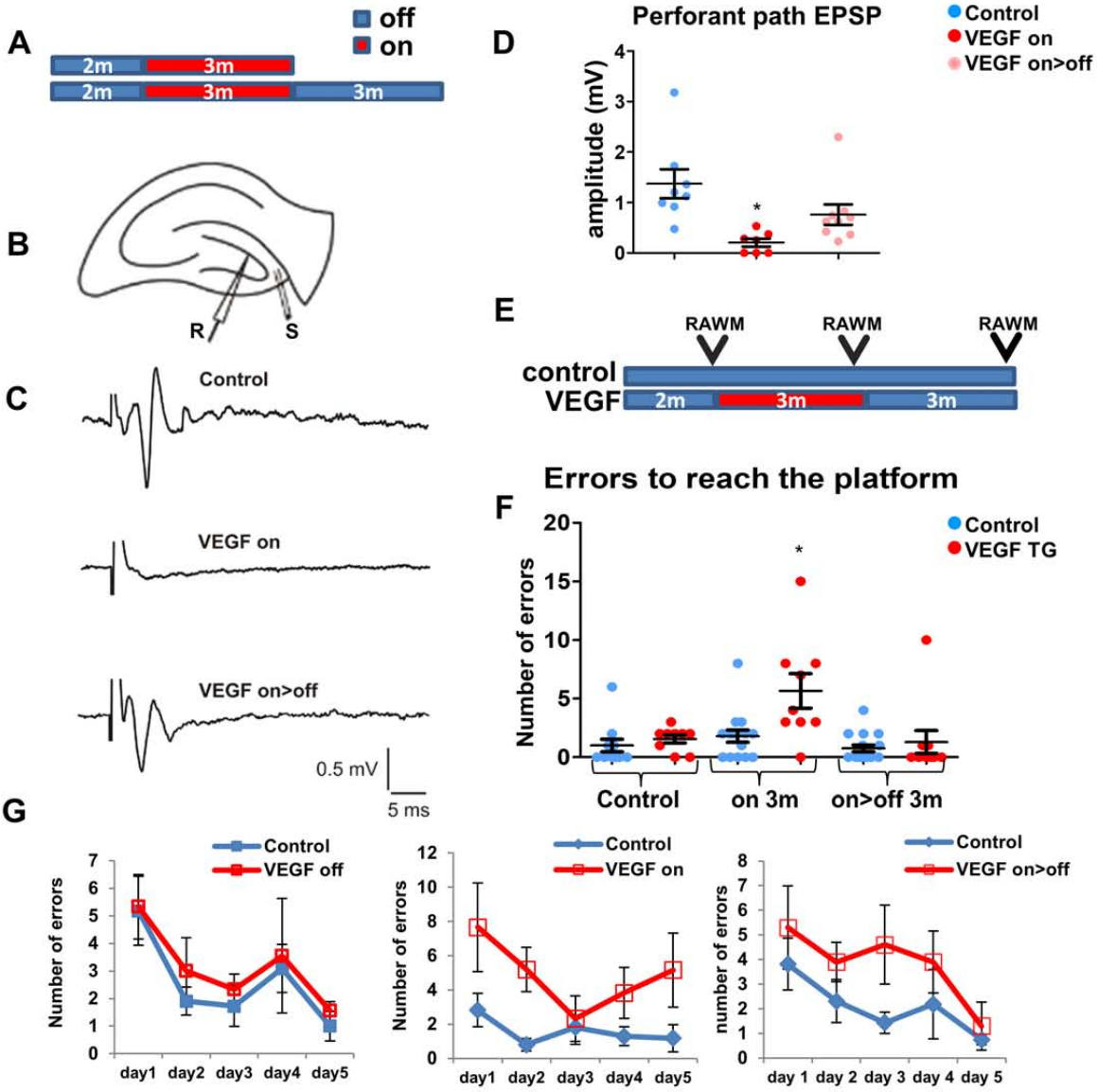

JNeurosci Accepted Manuscript

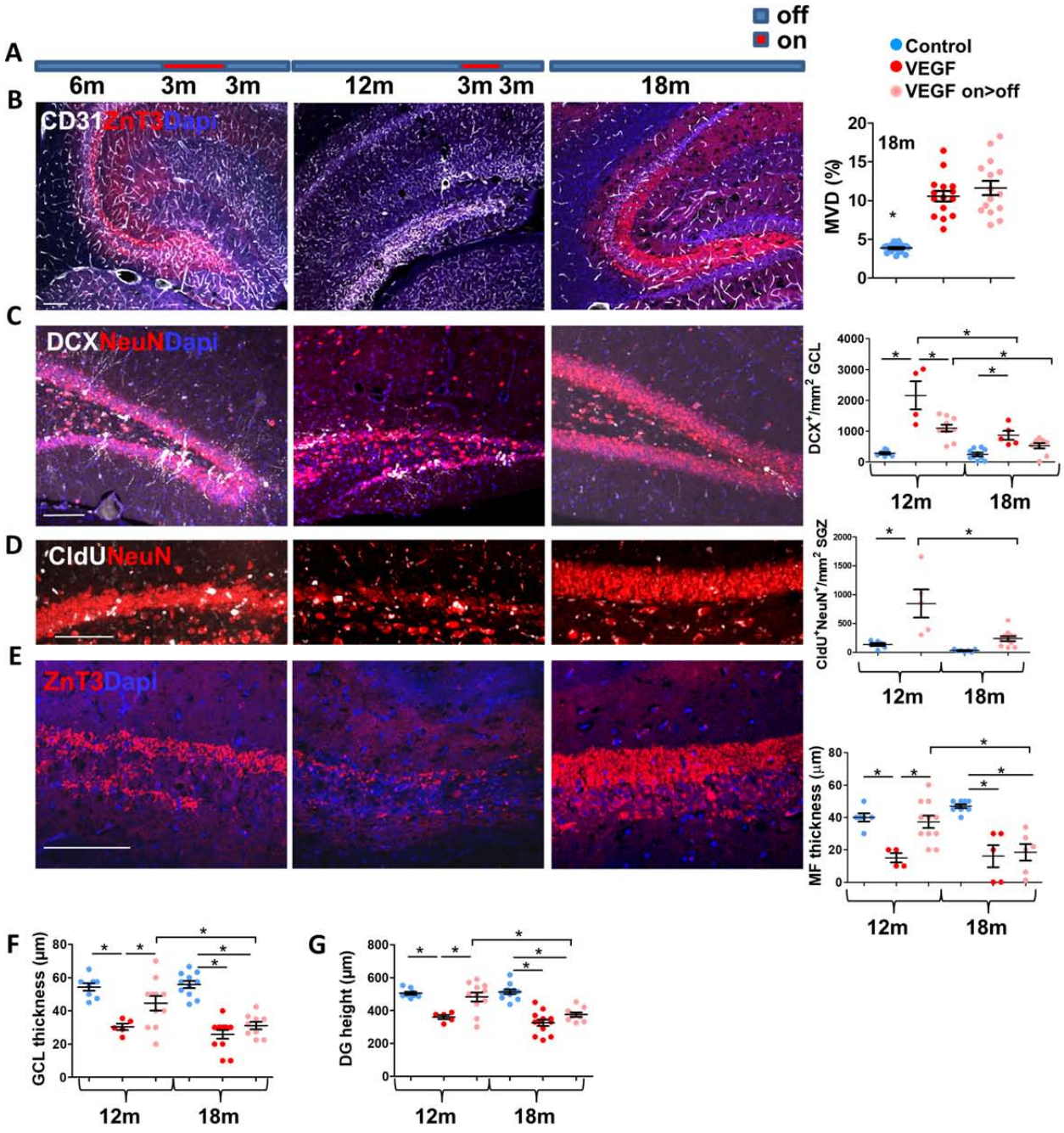

JNeurosci Accepted Manuscript

Figure	N	statistical test	F values main effect/T value	P value main effect	P value post hoc
1H DG height	Control: 6 20dpi: 7 90dpi: 5	1-way ANOVA	F(2,12)=16.508	$p=3.58*10^{-4}$	20dpi vs. Control: $p=2.54*10^{-4}$ 20dpi Vs. 90dpi: p=0.027
1H GCL thickness:	Control: 6 20dpi: 7 90dpi: 5	1-way ANOVA	F(2,12)=28.8	$p=2.62*10^{-5}$	20dpi vs. Control: $p=3.84*10^{-5}$. 20dpi Vs. 90dpi; $p=1.02*10^{-4}$.
1H MF thickness	Control: 6 20dpi: 5 90dpi: 3	1-way ANOVA	F(2,11)=44.908	$p=5.11*10^{-6}$	20dpi vs. Control: $p=4.61*10^{-6}$ 20 dpi Vs. 90dpi: $p=1.92*10^{-4}$
1H NeuN density	Control: 6 20dpi: 7 90dpi: 5	1-way ANOVA	F(2,12)=20.67	p=0.0002	20dpi vs. Control: p=0.004 20dpi vs 90dpi: p=0.0026
2B	Control: 10 20dpi: 13	t-test	T(21)=0.4254	p=0.6747	
2F active NSCs density	Control: 5 20dpi: 6	t-test	T(9)=5.800	p=0.0007	
2F Active NSCs fraction	Control: 5 20dpi: 6	t-test	T(9)=5.542	p=0.0015	
2F Total neuroblast density	Control: 5 20dpi: 6	t-test	T(9)=4.516	p=0.0027	
2F Early neuroblasts density	Control: 5 20dpi: 7	t-test	T(10)=4.883	p=0.0028	
2F early neuroblasts fraction	Control: 5 20dpi: 7	t-test	T(10)=1.140	p=0.837	
2H Newborn neuron density	Control: 5 90dpi: 6	t-test	T(9)=4.977	p=0.0025	
2H Neuron fraction/total CldU	Control: 5 90dpi: 6	t-test	T(9)=3.208	p=0.0125	
3C	**1m:** Control: 11 VEGF: 15 **2m:** Control: 11 VEGF: 15 **3m:**	2-way ANOVA	Treatment: F(1,158)=169.19 Time: F(5,158)=20.067 time-treatment interaction (control/VEGF)*time: F(5,158)=5.384	Treatment $P=9.26*10^{-27}$ Time: $P=1.82*10^{-15}$ Interaction: $p=1.339*10^{-4}$	Control vs. VEGF: 1 month: $p=5.82*10^{-4}$ 2 months $p=5.11*10^{-4}$ 3 months: p=0.008 4 months:

JNeurosci Accepted Manuscript

	Control: 14 VEGF: 13 **4m:** Control: 13 VEGF: 15 **5m:** Control: 15 VEGF: 18 **7m:** Control: 11 VEGF: 11				$p=9.48*10^{-9}$ 5 months: $p=1.74*10^{-6}$ 7 months: $p=3.17*10^{-7}$
3D	Control: 60 1m: 61 2m: 15 3m: 46 4m: 16 5m: 18 7m: 11	1-way ANOVA	F(6,225)=88.892	$p=1.39*10^{-6}$	Control vs. 2m: $p=4.2*10^{-06}$ Control vs. 3m: $p=1.45*10^{-22}$ Control vs. 4m: $p=1.53*10^{-19}$ Control vs. 5m: $p=8.32*10^{-18}$ Control vs. 7m: $p=5.75*10^{-34}$
4B	Control: 13 VEGF: 10	t-test	CA1: T(21) =-10.752 DG: T(21)=-8.237	CA1: $p=9.21*10^{-10}$ DG: $P=7.39*10^{-8}$	
4C	Control: 12 VEGF: 10	t-test	CA1 neuron density: T(20)= -0.047 CA1 height: T(20)=-3.63	CA1 neuron density: P=0.7 CA1 height: p=0.002	
5C	No transgene: 4 tTa only: 4 tTa-tetGFP: 5	1-way ANOVA	GCL thickness: F(2,12)=0.6605 DG height: F(2,12)=1.906	GCL thickness: p=0.5378 DG height: P=0.199	
6D NeuN density	Control: 8 VEGF on: 8 VEGF on>off: 8	1-way ANOVA	F(2, 21)= 61.526	$p=1.655*10^{-9}$	Control Vs VEGF On: $p=6.279*10^{-9}$ Control vs VEGF On>off: $p=2.11*10^{-6}$ VEGF On vs VEGF On>off: p=0.002
6D GCL thickness	Control: 18 VEGF on: 9 VEGF on>off: 16	1-way ANOVA	F(2,40)=23.589	$P=1.7*10^{-7}$	Control Vs VEGF On: $p=6.279*10^{-9}$ Control vs VEGF On>off: $p=2.11*10^{-6}$ VEGF on vs VEGF On>off: p=0.002
6D DG height	Control: 18 VEGF on: 9	1-way ANOVA	F(2,40)=30.116	$P=1.04*10^{-8}$	Control Vs VEGF on: $p=1.15*10^{-8}$

JNeurosci Accepted Manuscript

	VEGF on>off: 16				Control Vs. VEGF on>off: p=0.01. VEGF on Vs. VEGF on>off: $p=4.76*10^{-4}$
6D MF thickness	Control: 9 VEGF on: 9 VEGF on>off: 7	1-way ANOVA	F(2,19)=28.35	$p=1.9*10^{-6}$	Control vs On: $p=1.18*10^{-6}$ Control vs on>off: p=0.014 On vs On>off: p=0.01
6E	Same as 3D On>off 1m: 12 On>off 2m: 16 On>off 3m: 30	2-way ANOVA	Treatment: F(2,161)=207.169 Time: F(2,161)=11.382 Interaction: F(2,161)=27.373	Treatment: $p=2.99*10^{-45}$ Time: $p=2.37*10^{-5}$ Interaction: $p=5.84*10^{-11}$	Control vs 3m on>1m off: $4.83*10^{-13}$ Control vs 3m on>3m off: $p=1.65*10^{-4}$ 5m on vs.3m on>2m off: $p=4.83*10^{-13}$ 7m on vs. 3m on>3m off: $p=4.82*10^{-13}$
7D Total NSC density	Control: 11 VEGF on: 7 VEGF on>off: 13	1-way ANOVA	F(2, 28)=27.632	p=0.22	Control Vs VEGF On: p=0.019
7D active NSC density	Control: 11 VEGF on: 7 VEGF on>off: 13	1-way ANOVA	F(2,28)= 13.39	p=0.0002	Control Vs VEGF On: p=0.0002 Control Vs VEGF On>off: p=0.0002
7D fraction of active NSC	Control: 11 VEGF on: 7 VEGF on>off: 13	1-way ANOVA	F(2,28)=4.379	$p=2.26*10^{-7}$	Control Vs VEGF On: $p=4.24*10^{-7}$. Control Vs VEGF On Off: $p=2.03*10^{-5}$
8B	Control: 15 VEGF on: 7 VEGF on>off: 12	1-way ANOVA	F(2, 31)=50.405	$p=1.8*10^{-10}$	Control vs. VEGF On>off $p=5.47*10^{-9}$ VEGF on vs. VEGF On>off: $p=9.53*10^{-8}$
8C MVD	Control: 19 VEGF on: 8 VEGF on>off: 10	1-way ANOVA	F(2, 34)= 154.153	$p=1.84*10^{-9}$	Control Vs VEGF On: $p=3.33*10^{-7}$ Control vs VEGF on>off: $p=3.47*10^{-8}$
8C total neuroblast density	Control: 19 VEGF on: 7 VEGF on>off: 10	1-way ANOVA	F(2, 32)= 58.735	$p=1.9*10^{-11}$	Control Vs VEGF On: $p=5.208*10^{-9}$ Control vs VEGF on>off: $p=2.12*10^{-8}$
8D late neuroblast density	Control: 14 VEGF on: 6 VEGF on>off: 11	1-way ANOVA	F(2,28)=26.836	$p=3.09*10^{-7}$	Control vs. VEGF on $p=1.59*10^{-6}$ Control vs. VEGF on>off $p=1.69*10^{-5}$
8D late neuroblas	Control: 14 VEGF on: 6	1-way ANOVA	F(2,28)=6.084	p=0.006	Control vs. VEGF on>off p=0.01

JNeurosci Accepted Manuscript

t %	VEGF on>off: 11				VEGF on vs. VEGF on>off p=0.031
9D	Control: 8 VEGF on: 7 VEGF on>off: 9	1-way ANOVA	F(2,21)=6.808	p=0.005	Control vs. VEGF On: p=0.004 VEGF On>off vs. VEGF on: p=0.028
9F	Control: 15 VEGF: 9	2-way ANOVA	Treatment: F(1,64)=10.785 Time: F(2,64)=10.987 Time by treatment interaction F(2,64)=4.198	Treatment: p=0.002 Time: $p=7.9*10^{-5}$ Interaction: p=0.019	Control vs VEGF on: p=0.004
10B	Control: 18 VEGF on: 15 VEGF on>off: 15	1-way ANOVA	F(2, 45)=47.84	$p=7.27*10^{-12}$	Control vs VEGF On: $p=8.08*10^{-9}$ Control vs VEGF On>off: $p=5.15*10^{-9}$
10C 12m	Control: 7 VEGF on: 4 VEGF on>off: 10	1-way ANOVA	F(2,29)=34.5	$P=1.55*10^{-5}$	Control Vs VEGF On: $p=1.02*10^{-5}$; control vs. VEGF On>off: 0.005 VEGF On Vs. VEGF On>off: p=0.003
10C 18m	Control: 10 VEGF on: 5 VEGF on>off: 9	1-way ANOVA	F(2,21)=11.07	P=0.001	Control Vs VEGF On: $p=3.93*10^{-4}$ Control Vs. VEGF On>off: p=0.048
10C	12m vs 18m	2-way ANOVA	Treatment: F(2,39)=53.71 Age: F(1,39)=31.749 Interaction: F(2,39)=9.031	Treatment: $p=1.5*10^{-9}$ Age: $p=1.66*10^{-6}$ interaction: p=0.001	VEGF On 12m vs VEGF on 18m: $p=4.4*10^{-5}$ VEGF On>off 12m vs VEGF on>off 18m: p=0.015
10D	12m: Control: 6 VEGF on>off: 5 18m: Control: 7 VEGF on>off: 11	2-way ANOVA	Treatment: F(1,25)=25.164 Age: F(1,25)=15.171 Interaction: F(1,25)=7.44	Treatment: $p=3.57*10^{-5}$ Age: p=0.001 Interaction: p=0.011	12m Control vs. On>off: $p=2.31*10^{-4}$ 12m On>off vs 18m On>off: $p=3.83*10^{-4}$
10E 12m	Control: 6 VEGF on: 4 VEGF on>off: 11	1-way ANOVA	F(2,18)=8.338	p=0.003	Control Vs VEGF On: p=0.04 VEGF On Vs VEGF On-off :p=0.04
10E 18m	Control: 9 VEGF on: 5 VEGF on>off: 6	1-way ANOVA	F(2,17)=20.527	$p=2.9*10^{-5}$	Control Vs VEGF On: $p=1.37*10^{-5}$ Control Vs VEGF On-off: $p=1.85*10^{-4}$
10E	12m vs 18m	2-way ANOVA	Treatment: F(2,53)=34.516	Treatment: $p=2.25*10^{-10}$ Age: p=0.032	On>off 12m vs On>off 18m: p=0.0148

JNeurosci Accepted Manuscript

			Age: F(1,53)=3.672 Interaction: F(2,53)=3.166	interaction: p=0.021	
10F 12m	Control: 8 VEGF on: 5 VEGF on>off: 11	1-way ANOVA	F(2,21)=7.61	P=0.003	Control Vs VEGF On: p=0.002
10F 18m	Control: 11 VEGF on: 12 VEGF on>off: 9	1-way ANOVA	F(2,29)=46.408	$P=9.16*10^{-10}$	Control Vs VEGF On: $p=6.43*10^{-9}$ Control Vs. VEGF On>off: $p=3.06*10^{-7}$
10F	12m vs 18m	2-way ANOVA	Treatment: F(2,50)=36.843 Age: F(1,50)=4.529 Interaction: F(2,50)=3.192	Treatment: $p=1.466*10^{-10}$ Age: p=0.038 interaction: p=0.05	On>off 12m Vs On>off 18; p=0.025
10G 12m	Control: 8 VEGF on: 5 VEGF on>off: 11	1-way ANOVA	F(2,21)=8.175	P=0.002	Control Vs VEGF On: p=0.003 VEGF On Vs. VEGF On>off: p=0.007
10G 18m	Control: 11 VEGF on: 12 VEGF on>off: 9	1-way ANOVA	F(2,29)=34.5	$P=2.14*10^{-8}$	Control Vs VEGF On: $p=2.36*10^{-8}$ Control Vs. VEGF On>off: $p=1.62*10^{-5}$
10G	12m vs 18m	2-way ANOVA	Treatment: F(2,50)=30.784 Age F(1,50)=7.067 Interaction: F(2,50)=4.568	Treatment: $p=1.93*10^{-9}$ Age: p=0.011 interaction: p=0.015	On>off 12m vs On>off 18m: p=0.0035